JOURNAL OF PETROLOGY | VOLUME 48 | NUMBER 12 | PAGES 2289–2326 | 2007 | doi:10.1093/petrology/egm060

Large-scale Mechanical Redistribution of Orthopyroxene and Plagioclase in the Basement Sill, Ferrar Dolerites, McMurdo Dry Valleys, Antarctica: Petrological, Mineral-chemical and Field Evidence for Channelized Movement of Crystals and Melt

JEAN H. J. BÉDARD[1]*, BRUCE D. MARSH[2], TABER G. HERSUM[3], H. RICHARD NASLUND[4] AND SAMUEL B. MUKASA[5]

[1]GEOLOGICAL SURVEY OF CANADA—QUÉBEC OFFICE, 490 DE LA COURONNE, QUÉBEC CITY, QUÉBEC, CANADA, G1K 9A9

[2]JOHNS HOPKINS UNIVERSITY, DEPARTMENT OF EARTH AND PLANETARY SCIENCES, BALTIMORE, MD 21218, USA

[3]LAMONT–DOHERTY EARTH OBSERVATORY, PALISADES, NY 10964, USA

[4]SUNY BINGHAMTON, DEPARTMENT OF GEOLOGICAL SCIENCES, BINGHAMTON, NY 13902, USA

[5]DEPARTMENT OF GEOLOGICAL SCIENCES, UNIVERSITY OF MICHIGAN, 2534 C. C. LITTLE BLDG., 1100 N. UNIVERSITY AVE., ANN ARBOR, MI, 48109, USA

RECEIVED JANUARY 5, 2007; ACCEPTED SEPTEMBER 18, 2007
ADVANCE ACCESS PUBLICATION OCTOBER 25, 2007

The Jurassic Ferrar dolerite sills of the McMurdo Dry Valleys, Antarctica represent the plumbing system for flood basalt eruptions associated with the breakup of Gondwana. Among the Ferrar sills, the 350–450 m thick cumulate-textured Basement Sill is differentiated into a Lower Marginal Zone (LMZ) gabbronorite, a thick Lower Zone (LZ) orthopyroxene–plagioclase orthocumulate pyroxenite, a strongly layered mela- to leuco-gabbronorite Middle Zone (MZ), a thick Upper Zone (UZ) gabbronorite with ferrogabbroic pods, and an Upper Marginal Zone (UMZ) gabbronorite. Textures and mineral compositions in the LZ pyroxenite and MZ–UZ gabbronorites are nearly identical, the main distinction being the greater relative proportion of plagioclase in the MZ–UZ gabbronorites, and of pigeonite in the UZ. Most orthopyroxene in the LZ, MZ and UZ occurs as sub-euhedral, normally zoned primocrysts, commonly with rounded plagioclase inclusions. Plagioclase is usually sub-euhedral and normally zoned, but can contain sodic cores interpreted to be xenocrystic. Orthopyroxene and feldspar compositions thoughout the sill are generally fairly uniform, and resemble the compositions of micro-phenocrysts in the chilled margins. We infer that the sill was filled by a c. 1250°C slurry of orthopyroxene + plagioclase phenocrysts or primocrysts that subsequently unmixed in response to buoyancy forces. The LZ websterite contains numerous anorthosite to gabbronorite schlieren, veins and pipes (<2 m diameter), which we interpret as fossil segregation channels. Textures and mineral compositions in these felsic channels are very similar both to UZ and MZ gabbronorites, and to the groundmass separating accumulated orthopyroxene primocrysts in the LZ and MZ. We infer that plagioclase-charged, hydrous pore melt from the pyroxenite may have segregated, pooled and ascended through these conduits to feed growth of the UZ gabbronorite. Detailed mapping shows that the pipes are separated by about 15 m on average. Calculations suggest that this number density of conduits could have drained the LZ cumulates of their interstitial melt + plagioclase in about 8 days. Sequences (each c. *5–10 m thick) of layered leuco-gabbronorite in the MZ could represent*

*Corresponding author. E-mail: jbedard@rncan.gc.ca

intra-cumulate sills that formed from plagioclase-rich slurries ascending in segregation channels. Fe–Ti-rich pyroxenitic veins and pods (some pegmatitic) and an unusual coarse-grained plagioclase facies occur at the contacts between massive leuco-gabbronorite layers in the MZ. Discordant ferro-pegmatite pods and dykes occur throughout the UZ. We interpret these Fe-rich pegmatoidal rocks as evolved residual melts expelled from the compacting gabbronoritic cumulates of the MZ and UZ.

KEY WORDS: *Ferrar; cumulates; differentiation; Antarctica; layering*

INTRODUCTION

There is considerable uncertainty with regard to how crystal concentrations (cumulates) form in layered intrusions. Gravity-driven mechanisms were favoured by Wager & Deer (1939) and many others (e.g. Irvine, 1980, 1987; Martin & Nokes, 1989; see discussion by Naslund & McBirney, 1996), but *in situ* crystallization processes are also commonly proposed (e.g. Hess, 1939; McBirney & Noyes, 1979; Campbell, 1987). One reason why it is so difficult to determine how cumulate rocks form is that in many large, slowly cooled layered intrusions, post-cumulus re-equilibration obscures the textural and mineral-chemical evidence (Boudreau, 1987; Hunter, 1987; Bédard *et al.*, 1988; Bédard, 1989). The lowermost of the Jurassic Ferrar sills of Antarctica (Basement Sill, Figs 1 and 2), contains a well-developed sequence of pyroxenitic and gabbroic rocks. Because of its modest thickness (<450 m) the Basement Sill cooled rapidly, so that the early magmatic textures and internal structures are well preserved, recording evidence for how the crystals formed and were concentrated, and for channelized post-cumulus migration of melt and crystals. The detailed study of field relations, petrography and mineral chemistry reported here allows us to postulate the action of dynamic and gravity-driven mechanisms by which large-scale mechanical separation of pyroxene and feldspar occurred in this sill, so generating the first-order lithological differentiation (pyroxenite base, gabbronorite top) that is observed. The data also indicate that residual melts enriched in SiO_2–FeO–TiO_2–Na_2O–K_2O–H_2O were expelled from the gabbronoritic cumulates to form pegmatoidal ferrogabbroic facies.

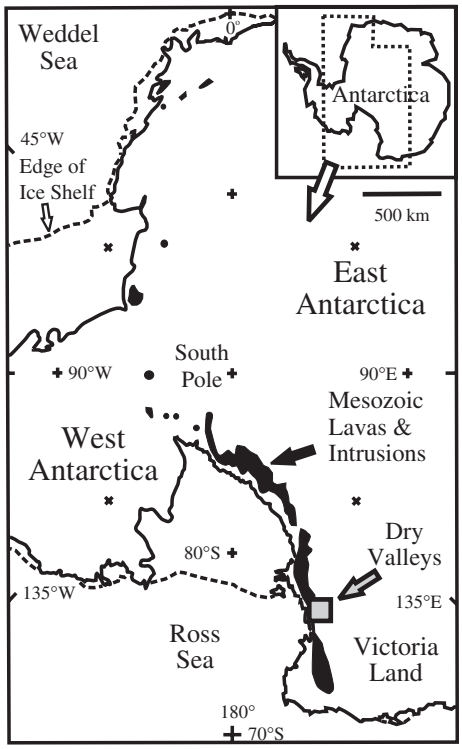

Fig. 1. Map showing the location of the Dry Valleys, Antarctica.

THE FERRAR DOLERITE SILLS, AND THE BASEMENT SILL

The Ferrar dolerite sills of the McMurdo Dry Valleys, Antarctica (Figs 1 and 2) are the hypabyssal equivalent to the Kirkpatrick Basalts, a continental flood basalt suite related to the Mesozoic breakup of Gondwanaland that is penecontemporaneous with the Karroo cycle of South Africa (Hergt *et al.*, 1991; Elliot & Fleming, 2000; Zhang *et al.*, 2003). The Kirkpatrick Basalts are dominated by the SiO_2-rich, TiO_2-poor Mt. Fazio Lava Series (MFLS, Elliot, 1992; Elliot *et al.*, 1995; Fleming *et al.*, 1995), which has trace element and isotopic signatures [$^{87/86}Sr_i > 0{\cdot}71$, negative Nb–Ta–Ti anomalies, large ion lithophile element (LILE) enrichment, Zr–Th enrichment] indicating either extensive crustal contamination, or derivation from supra-subduction-zone metasomatized continental lithosphere (Kyle, 1980; Elliott *et al.*, 1995; Fleming *et al.*, 1995; Elliot & Fleming, 2000). The geology of the pre-Mesozoic sequence in Antarctica has been reviewed by Fleming *et al.* (1995), Stump (1995) and Storey *et al.* (1996).

There are four Ferrar sills in the McMurdo Dry Valleys Region of the Trans-Antarctic Mountains (Figs 1 and 2). From top to bottom, these are the Mt. Fleming, Asgard, Peneplain and Basement Sills (Marsh, 2004). The three upper sills were emplaced into Permian to Jurassic age Beacon Supergroup sediments (Hamilton & Hayes, 1965), which immediately underlie the Kirkpatrick Basalts (Elliot, 2000). The three upper sills are up to 433 m thick (Gunn, 1966) and, like many such hypabyssal, pigeonite-bearing, tholeiitic bodies, are characterized by doleritic to sub-ophitic textures, with near-liquid compositions attesting to the limited extent to which crystal–liquid segregation processes were able to act in these fast-cooling sub-volcanic intrusions (Gunn, 1966). In contrast, the Basement Sill was emplaced into the underlying orogenic Cambro-Ordovician granitoids (Stump, 1995) and exhibits

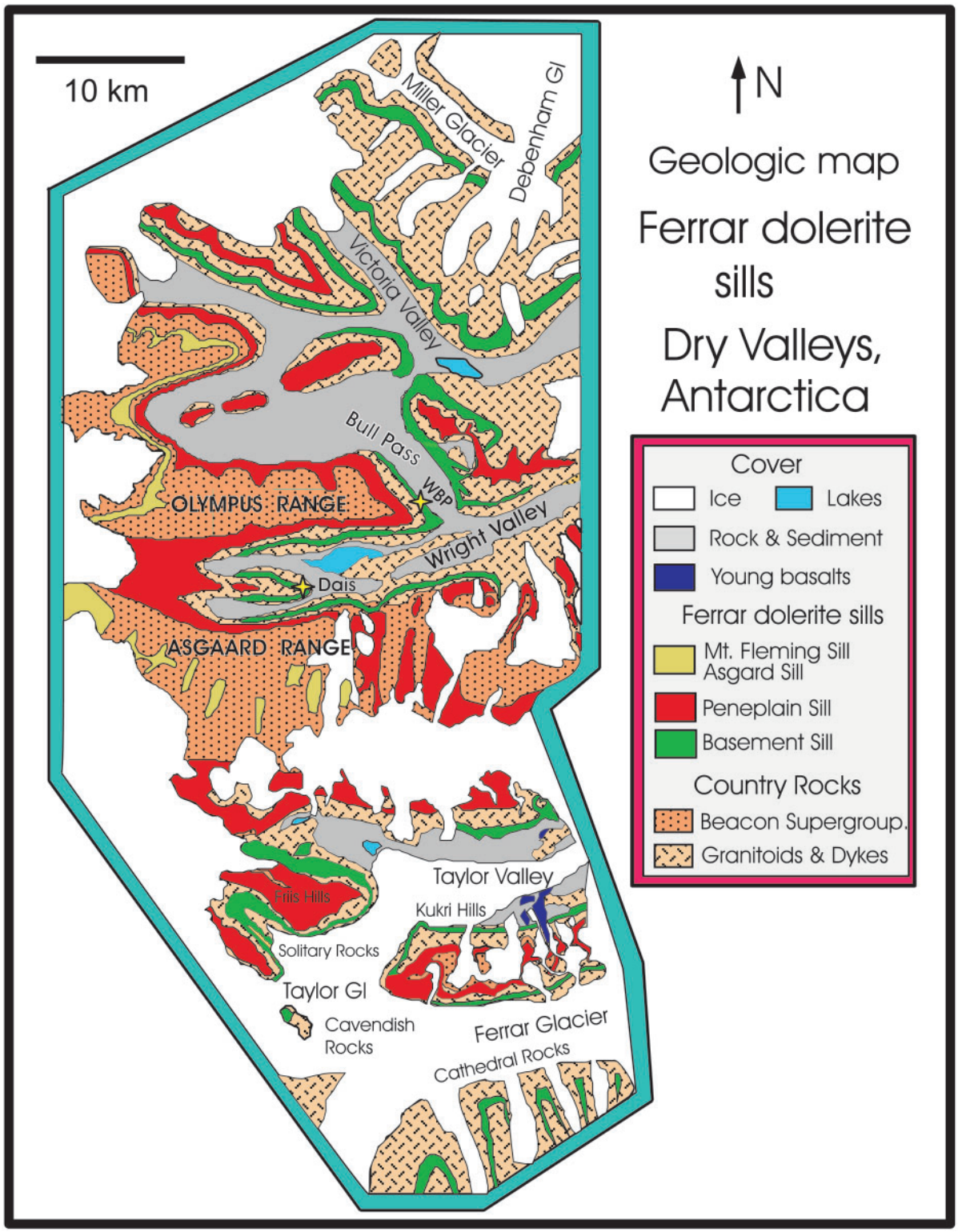

Fig. 2. Geological map of the Dry Valleys area, adapted from Marsh & Zieg (unpublished work). Dais, Dais Intrusion (Basement Sill); WBP, West Bull Pass.

cumulate textures similar to those seen in large layered intrusions, with an orthopyroxene-enriched base that has been referred to as an 'orthopyroxenite tongue' hitherto (Figs 3 and 4: Gunn, 1966; Marsh, 2004; Charrier & Marsh, 2004, 2005).

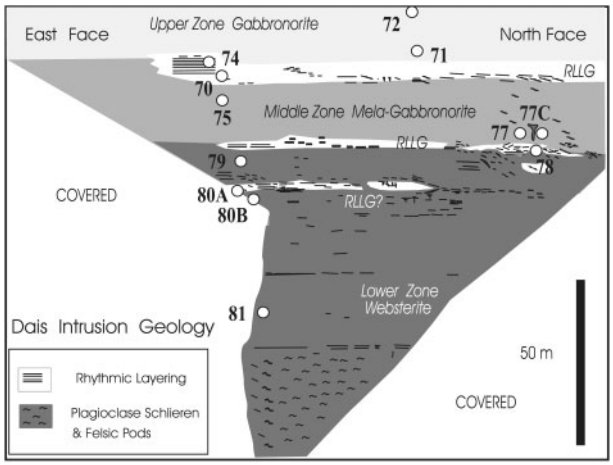

Fig. 3. Generalized sketch section of the central portion of the Dais Intrusion, showing the distribution of different types of felsic segregations and samples. RLLG, rhythmically layered leuco-gabbronorite sequences (see text).

Although the Basement Sill is a single body that has been traced out in three dimensions over the entire McMurdo Dry Valleys (Fig. 2), its lobate form shows considerable variations in shape, thickness and level of emplacement. Field data (Marsh *et al.*, 2005) imply that the Basement Sill dips and thickens inward towards a focus in the West Bull Pass area (WBP), which was interpreted to be near the main magma ascent and filling point (Marsh *et al.*, 2005). The lowermost lobe of the Basement Sill crops out in the base of Wright Valley and is known as the Dais Intrusion (Marsh, 2004). The upper contact of the Dais Intrusion is at about 600 m altitude, but only the upper two-thirds or so (~450 m) of the sill is exposed there. Along the north side of Wright Valley, the Basement Sill has a uniform thickness and attitude, with a base at *c.* 650 m altitude. Along the south wall of Wright Valley, the Basement Sill forms several large coalescent lobes that climb upward and quench against the Peneplain Sill. As the Basement Sill continues north and south at an even thickness of ~350 m outward from the WBP and Dais areas for up to 50 km, the pyroxenite tongue systematically thins and eventually pinches out in the most distant parts of the sill (Marsh, 2004; Charrier & Marsh, 2004). To the east along Wright Valley,

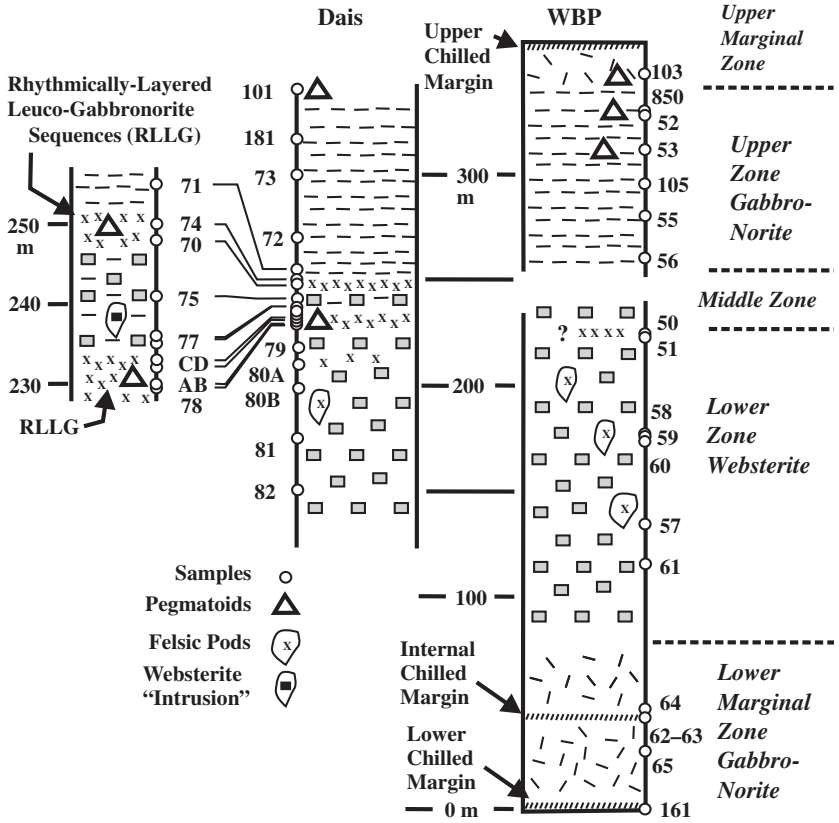

Fig. 4. Stratigraphic sections of the Dais and West Bull Pass lobes of the Basement Sill, showing sample positions.

the Basement Sill thins to a centimeter-sized chilled dolerite vein.

INTERNAL STRATIGRAPHY OF THE BASEMENT SILL

Two broadly similar, and generally well-exposed sections were sampled (Dais and WBP: Figs 2–4). Sample locations were constrained with a global positioning system (Electronic Appendix 1, Table A1-2, available for downloading from http://www.petrology.oxfordjournals.org), and transformed to x–y coordinates with a polar azimuthal projection. Stratigraphic positions in the Dais section were corrected for a 5° southward dip. A single sample from the south wall of Wright Valley (sample 181) was interpolated into the Dais stratigraphy. The detailed mineralogy of each of the samples is given in Electronic Appendix 1, Table A1-1.

Lower Marginal Zone (LMZ)

In the WBP area, a black, 10 cm thick aphanitic, microporphyritic lower chilled margin (sample 161, 6·4% MgO) coarsens rapidly inward into a massive, fine- to medium-grained gabbro-norite (samples 64 and 65, <70 m thick) that constitutes the Lower Marginal Zone (LMZ). Internal fine-grained contacts (samples 62 and 63) suggest that the LMZ records more than one pulse of magma, albeit with similar compositions. As the size and proportion of orthopyroxene primocrysts increase up-section, the LMZ gabbronorite grades up into Lower Zone websterite. Gunn (1966) observed sharp transitions on a 1–2 m scale.

Lower Zone (LZ) or pyroxenite tongue

Most of the Lower Zone (<170 m thick) is composed of feldspathic websterite and mela-gabbronorite (for simplicity, we will refer to these rocks as websterites henceforth), with feldspathic segregations on various scales. In places the websterite appears completely massive, commonly with a preferred orientation of orthopyroxene that is subparallel to the base of the sill. Centimeter-sized leuco-gabbronorite clots are locally present. Discontinuous and ramifying millimeter- to centimeter-thick anorthositic to leuco-gabbronorite schlieren or veins are common (Fig. 5a and b). These can be closely (2–5 cm), or widely (m) spaced, and oriented parallel or perpendicular to the sill contacts. In places, there is evidence for boudinage and plastic deformation (Fig. 5c). Decimeter-sized felsic veins resemble complex stockworks (Fig. 5d). Thicker felsic bodies (0·5–2 m) sometimes occur as laterally continuous

Fig. 5. Field photographs of the Websterite Zone. White arrows indicate 'up' direction. (a) Sequence of pseudo-rhythmically layered anorthositic schlieren in Dais LZ websterite. Branching of schlieren (black arrow) should be noted. Pole is 1·5 m in length. (b) Close-up of anorthositic schlieren (*c.* 1 cm wide) in Dais LZ websterite. (c) Plastically deformed feldspathic layers in WBP LZ websterite. Shear bands should be noted. (d) Channeled segregations in Dais LZ websterite with anorthositic bases (a) and a gabbronoritic top (g). It should be noted that felsic layers branch, and that there are isolated euhedral orthopyroxene phenocrysts in the feldspathic channels.

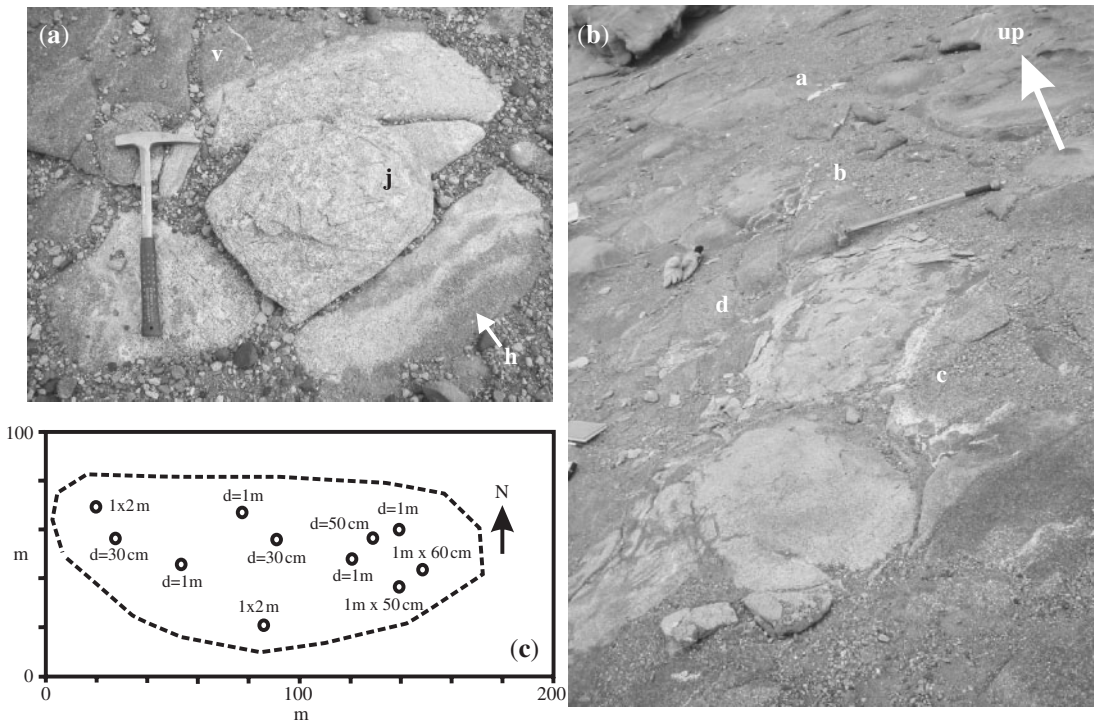

Fig. 6. Feldspathic pods and schlieren in WBP LZ websterite. (a) Pod 57 has a coarse, jackstraw-textured leuco-gabbronorite core (j, sample 57B, see Fig. 18a) and a finer-grained, more feldspathic rim. The narrow anorthositic apophyses (v, sample 57C) that appear to be rooted in the host websterite (sample 57A, see Fig. 18c), and the complex 'hybrid' zone on one side (h), should be noted. Hammer is 30 cm long. (b) Pod 59 has a gabbronoritic core (sample 59A, see Fig. 18d), grading to anorthositic gabbronorite at the contact (c) that is rooted (d) in the host websterite. The distal anorthositic veinlets or schlieren (a and b, sample 59B) should be noted. Sledgehammer is *c.* 1 m long. (c). Detail map from a bench (subparallel to bedding) in the upper part of the WBP LZ. The surface area used to determine the pipe number density is shown as a dashed line. Only pipes larger than 30 cm were measured. d, diameter.

layers (over tens of meters), forming a series of lenses at the same stratigraphic level (Fig. 3). Other felsic bodies are ovoid in shape (maximum diameter 2 m) and can be elongated in the paleo-vertical direction (Fig. 6). Thicker felsic bodies commonly show internal lithological zoning, with jackstraw- to granular-textured gabbronorite cores, and concentrically foliated leuco-gabbronorite to anorthosite margins (Figs 5d and 6). The margins connect to smaller anorthositic schlieren or veins that appear to be rooted in the host websterite (Fig. 6). In places, the coarse orthopyroxene primocrysts characteristic of the websterite appear to be entrained into these diverse felsic bodies (Fig. 5b and d).

Middle Zone (MZ)

In the Dais Intrusion, the Middle Zone separates Lower Zone websterite from Upper Zone gabbronorite. It includes the two highest contact-parallel sequences of rhythmically layered leuco-gabbronorite (RLLG in Figs 3, 4 and 7a), each *c.* 5–12 m thick, and separated by *c.* 20–25 m of mela-gabbronorite (samples 75, 77A and 77B) that is slightly more feldspathic than typical LZ websterite. Discontinuous layered leuco-gabbronorites embedded in the underlying LZ websterite (e.g. samples 50 and 80A) are very similar to MZ leuco-gabbronorites, but are grouped with the LZ. A vertically elongated, 2 m × 1 m sized, websteritic intrusive body (sample 77C, Fig. 7b) has crenulated, lobate contacts against host MZ mela-gabbronorite (sample 77B proximal, sample 77A distal) on one side, whereas the other side has a contact that is brecciated and veined (1–3 cm) by anorthosite (sample 77D).

The two MZ layered leuco-gabbronorite sequences in the Dais Intrusion are similar. They are dominated by massive, 0·5–3 m thick layers of gabbronorite to leuco-gabbronorite, with a prominent layering-parallel foliation developed in plagioclase and prismatic pyroxene (Naslund *et al.*, 2005). Orthopyroxene grain-size locally coarsens inward from both upper and lower contacts of these massive layers. Pyroxene-enriched schlieren and coarse plagioclase locally decorate contacts (Fig. 7a), and thicken laterally into meter-scale, locally pegmatoidal, ferro-gabbroic pods and veins that cross-cut layering (Fig. 7d). Micro-rhythmically layered gabbronorite is similar to the thick-bedded foliated leuco-gabbronorite, except for a higher pyroxene/plagioclase ratio, and centimeter-scale, laterally discontinuous, finer-grained, pyroxene-enriched layers.

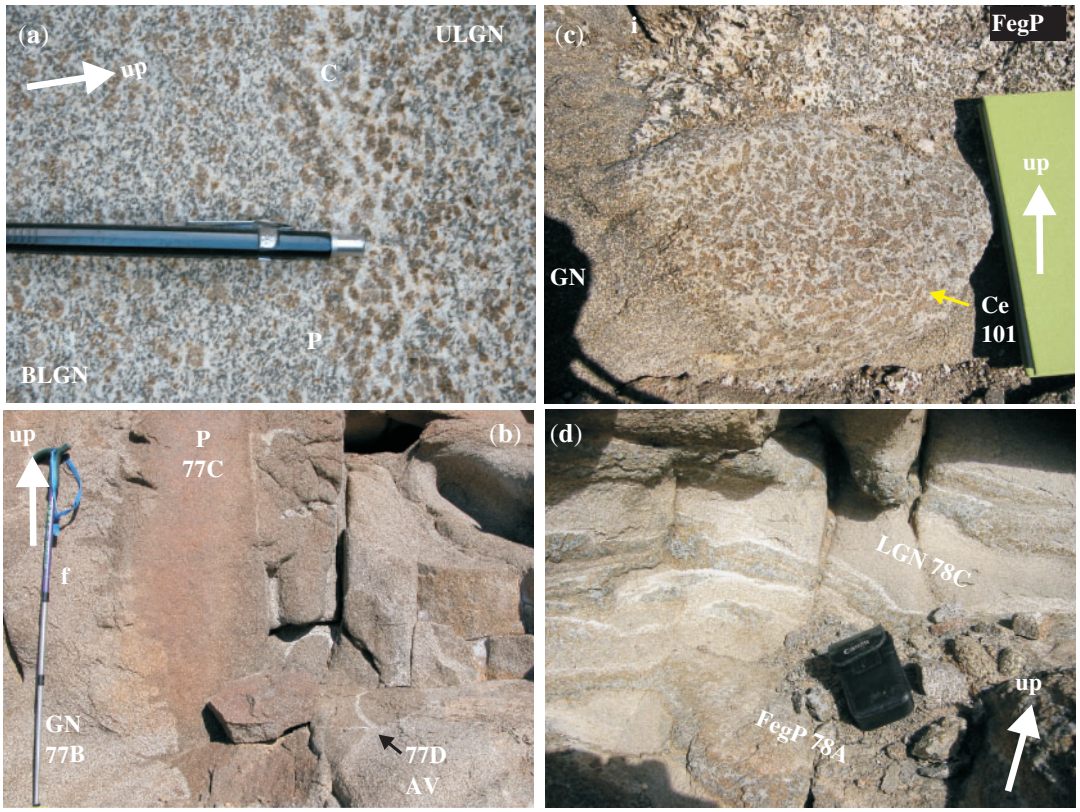

Fig. 7. (a) Rhythmically layered leuco-gabbronorite sequence corresponding to samples 70A and B from the Dais MZ. BLGN and ULGN are the basal and upper leuco-gabbronorite beds, respectively. The concentration of pyroxene (P) and the cellular-plagioclase layer (C) at the contact should be noted. Pen for scale. (b) Websterite pod (P 77C) embedded in a mela-gabbronorite (GN 77B) about 1 m above the top of the Dais MZ layered leuco-gabbronorite sequence (sample 78, Fig. 7d). The fingered contact (f) on one side, and the presence of anorthositic veinlets on the opposite side (AV 77D), should be noted. Pole is about 1·5 m high. (c) Pegmatoidal ferrogabbro pod from the upper part of Dais UZ. The inward-growth textures (i) should be noted. The base of the pod is occupied by an incipient cellular textured plagioclase layer (sample Ce 101). Height of photograph is ~25 cm. (d) Rhythmically layered leuco-gabbronorite interval in Dais MZ (LGN 78C). Host leuco-gabbronorites are cut by irregularly anastomosing pegmatoidal ferrogabbroic dykes (dark layers, FegP 78A) with anorthositic haloes. Camera case is 10 cm long.

At WBP, the interval corresponding to the MZ is poorly exposed, but thick rhythmically layered leuco-gabbronorite sequences appear to be lacking. Conversely, the upper 100 m of the Lower Zone at WBP contains abundant feldspathic layers and pods, spaced *c.* 15 m apart on average (Fig. 6).

Upper Zone (UZ)

The Upper Zone (UZ) is about 100 m thick (Fig. 4) and is dominated by foliated, medium-grained, porphyritic gabbronorite, hypidiomorphic gabbronorite with abundant inverted pigeonite, and ferrogabbroic pegmatoids. Most outcrops appear massive, but wispy, poorly defined rhythmic layering is observed locally. Ferrogabbroic pegmatoids (centimeters to 2 m in size) mainly occur as discrete, discordant pipes (Fig. 7c, Geist *et al.*, 2005), but also form wider 'stratiform' domains (extending up to 20 m along-strike and up to 5 m thick). Field observations suggest that the 'stratiform' ferrogabbros are constituted of closely spaced intrusive pipes that have spread out and merged laterally with the adjacent host gabbro. Pegmatoids commonly show inward-growth textures, with coarse prismatic clinopyroxene nucleated against their outer contacts. A few are zoned, with a 10 cm thick base constituted of ferrogabbro with a distinct texture (Fig. 7c). In places, the common UZ gabbronorite is decorated with dark 'rosettes' (sample 18l) composed of brown (in thin section) alteration veinlets. Single rosettes can be up to 10 cm wide, but are rarely more than 1 cm thick. They occur as sets (up to four) oriented along planes, suggesting growth after attainment of rigidity in the solidifying cumulus pile. The dark rosettes are interpreted to have formed during movement of deuteric fluids through the solidifying crystal mush.

Upper Marginal Zone (UMZ)

The Upper Marginal Zone is characterized by an irregular upper chilled margin that invades and mixes with

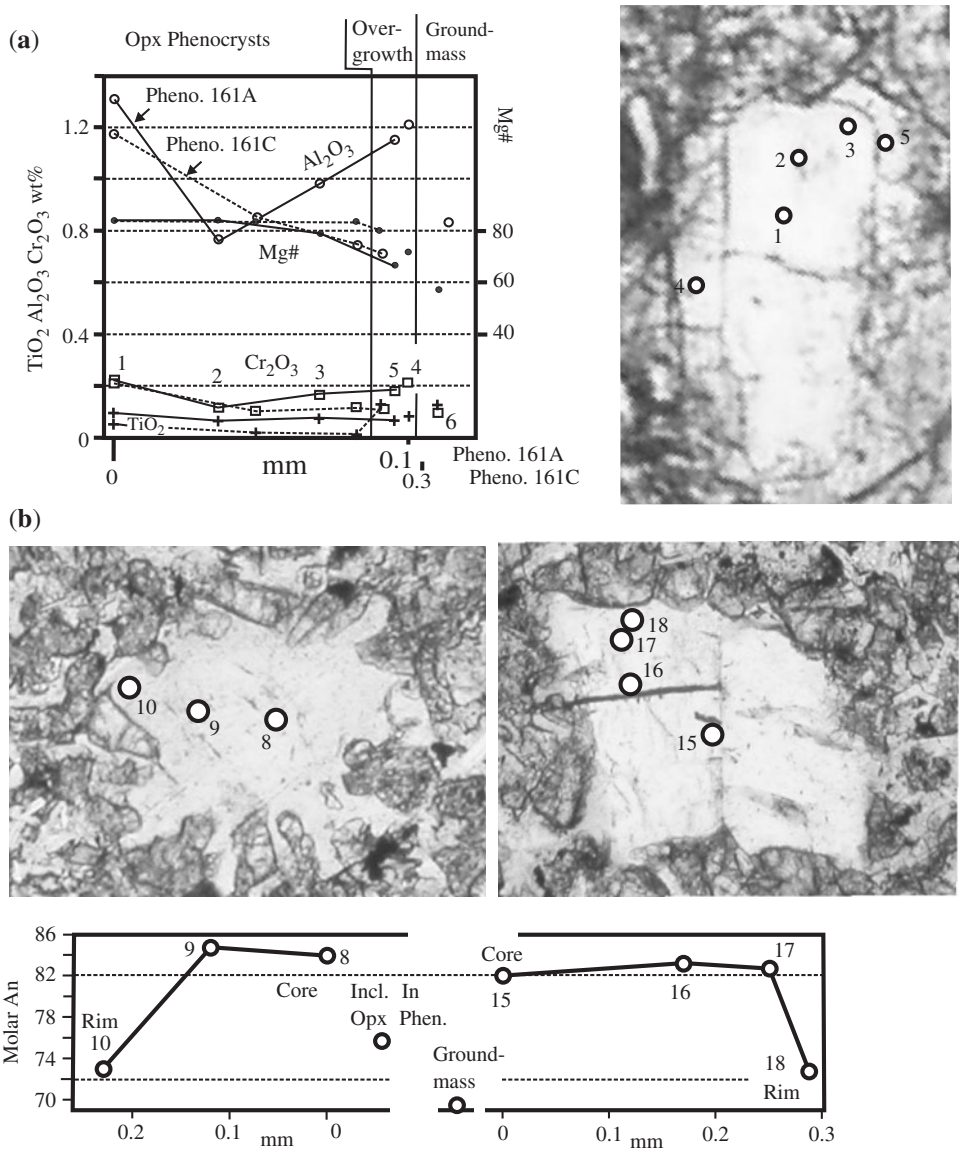

Fig. 8. Lower chilled margin WBP LMZ, sample 161. (a) Micrograph of micro-phenocryst 161 A (*c.* 0·12 mm long) and corresponding microprobe traverse. Numbers adjacent to spots are analysis numbers. The existence of an overgrowth (samples 5 and 4) on the euhedral prismatic micro-phenocryst should be noted. A second micro-phenocryst traverse is also shown (161 C). Both show gentle outward decrease of Mg-number, with complex patterns for Cr_2O_3 and Al_2O_3. (Note the difference in the bottom scale for the two traverses.) (b) Probe traverses and corresponding micrographs for two plagioclase micro-phenocrysts. Both have high-An cores, and sodic rims similar to groundmass compositions.

remobilized host granite. Facies located more than a few meters from the actual contact seem to be finer-grained equivalents of the UZ gabbronorites, and are very similar to the LMZ gabbronorites.

PETROGRAPHY AND MINERAL CHEMISTRY

Mineral chemical data are presented in the Electronic Appendices (Tables A2A–A2I), along with details of the pertinent analytical conditions.

Lower Marginal Zone (LMZ)

Chilled margin

The micro-diabasic lower chilled margin (sample 161, 6·4% MgO) contains micro-phenocrysts of normally zoned orthopyroxene (Fig. 8a) with core compositions (Mg-number <84·4) similar to those of orthopyroxene primocrysts from the LZ (see below, Fig. 15), and that contain tiny plagioclase inclusions. Micro-phenocrysts of normally zoned calcic plagioclase (<An84·7, Fig. 8b) have compositions similar to those of feldspar from the LZ, MZ and UZ (see below, Fig. 16).

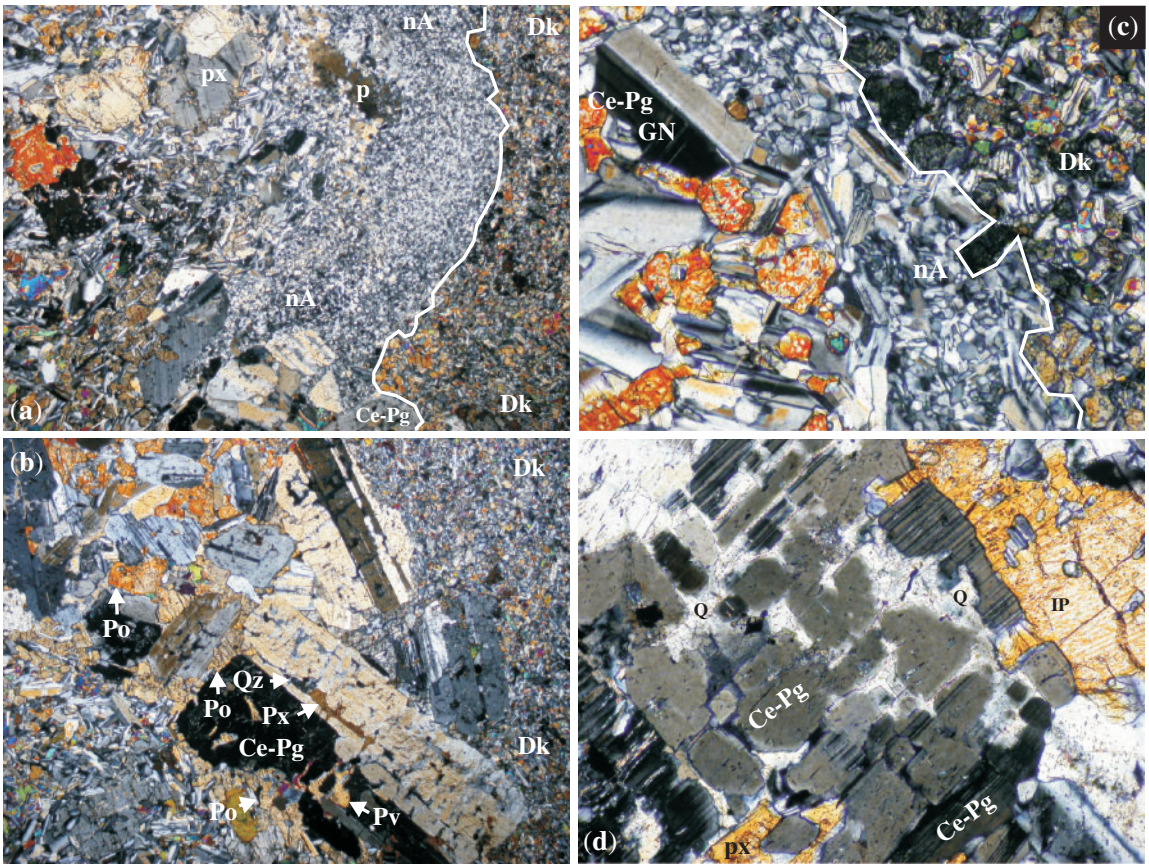

Fig. 9. Internal dyke contact, WBP LMZ, sample 63-2. (a) GN, gabbronorite; Dk, fine-grained dyke. The contact zone is characterized by the development of cellular-textured plagioclase (Ce-Pg), granular orthopyroxene (px), and an anorthositic band with variable development of a neoblastic mosaic (nA). The presence of relict plagioclase porphyroclasts (p) in the neoblastic matrix, and of plagioclase laths along the contact with the gabbronorite, should be noted. Field of view is 5 mm; crossed Nicols. (b) Contact between gabbronorite (GN) and dyke (Dk) characterized by the development of cellular-textured plagioclase (Ce-Pg), dissected by composite veinlets of quartz (Qz) and pyroxene (Px), one of which is in optical continuity (Pv) with larger, enveloping oikocrysts (Po). Field of view is 5 mm; crossed Nicols. (c). Contact between gabbronorite (GN) and dyke (Dk), characterized by the development of a neoblastic anorthositic band (nA). Field of view is 1·2 mm; crossed Nicols. (d) Cellular-textured plagioclase domain (Ce-Pg), with characteristic development of quartz + pyroxene + orthoclase + ilmenite + mica veinlets (Q). A large inverted pigeonite oikocryst (IP) above and to the right protrudes into the cellular-plagioclase, as does a smaller pyroxene (px) at the bottom. The re-equilibrated sodic haloes in the cellular-plagioclase adjacent to the quartz veins should be noted. Field of view is ~1·2 mm; crossed Nicols.

Gabbronorite

Fine- to medium-grained gabbronorites (average 0·5–1 mm) from the LMZ (samples 64 and 65) have hypidiomorphic textures with rare, euhedral, zoned plagioclase 'phenocrysts' (<2 mm, An <85·5), and abundant smaller laths. Sub-euhedral, normally zoned, prismatic orthopyroxene grains (<2 mm, Mg-number <83) contain tiny plagioclase laths. Inverted pigeonite is intergrown with, or forms rims on, both ortho- and clinopyroxene, and also occurs as interstitial or oikocrystic patches. Clinopyroxene occurs as sub-ophitic patches, as oikocrysts, or as larger ragged prisms (<2 mm), and is more Fe-rich than clinopyroxene from LZ websterites (see below, Fig. 17). Minor groundmass quartz, biotite and ilmenite are present.

Internal intrusive contacts

A fine-grained, micro-phyric internal intrusive contact cross-cuts LMZ gabbronorites (samples 62 and 63, Fig. 9), but does not preserve liquid compositions, having a clear 'cumulus' geochemical signature (unpublished data). The fine-grained contact rock contains rare prismatic, evolved orthopyroxene micro-phenocrysts (Opx Mg-number <73), and sparse, euhedral, normally zoned plagioclase micro-phenocrysts (An <86·6). The irregular contact is generally a sharp interface against LMZ gabbronorite (Fig. 9b), but locally host and intrusion are separated by a discontinuous 2 mm thick cellular-textured plagioclase domain (defined below Fig. 9b and d), which is locally separated from the internal contact rock by a neoblastic anorthosite domain up to 1 mm thick (Fig. 9a and c).

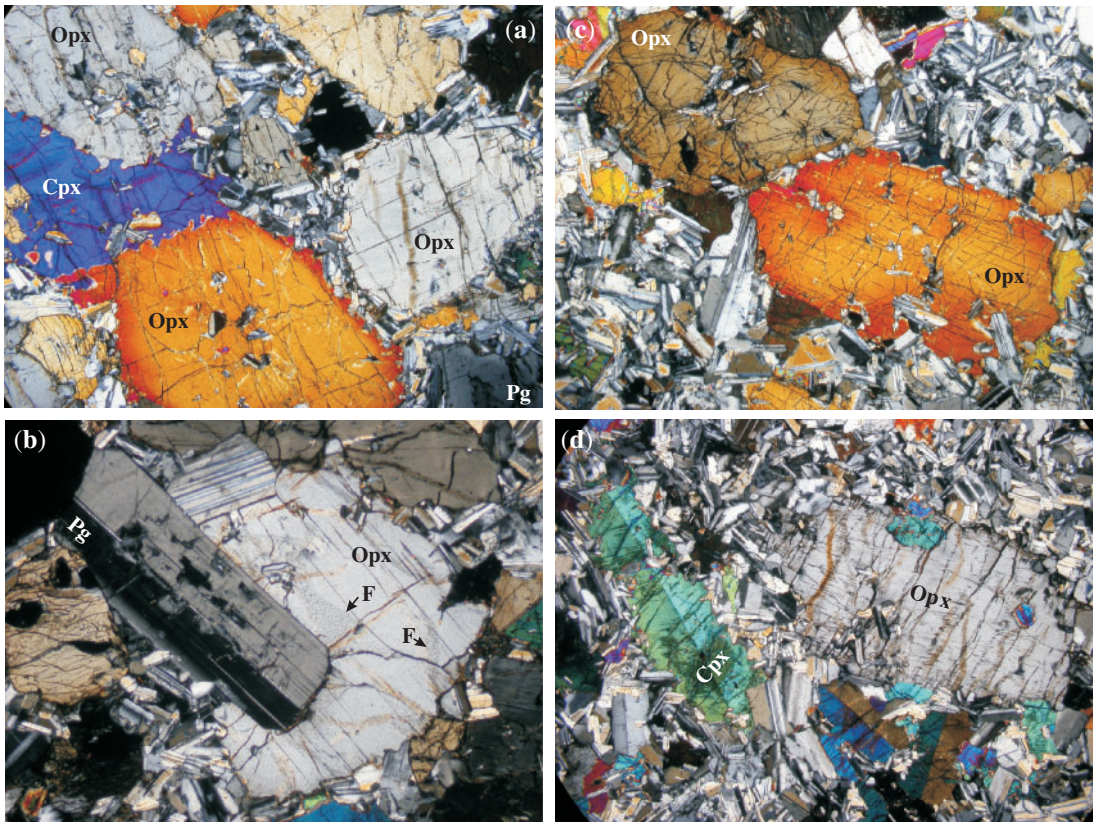

Fig. 10. Comparison of textures from main facies of LZ, MZ and UZ. Photomicrographs in (a), (c) and (d) are at the same scale; crossed Nicols for all images. (a) WBP LZ websterite 51. Euhedral orthopyroxene primocrysts (Opx) contain tiny plagioclase inclusions, and are separated by tiny groundmass plagioclase laths. The plagioclase grains trapped between sutured orthopyroxene primocrysts, the late interstitial clinopyroxene (Cpx) replacing the edges of orthopyroxene, and the complexly zoned plagioclase phenocryst at bottom right (Pg) should be noted. Field of view is 6 mm. (b) WBP LZ websterite 61. A large euhedral phenocryst of plagioclase (Pg) with a sodic inner core and clinopyroxene inclusions or veins is embedded in an orthopyroxene (Opx) primocryst. F, fluid–melt inclusion trails in orthopyroxene. Field of view is 4 mm. (c) Dais Intrusion MZ mela-gabbronorite 75, from a septum separating two layered leuco-gabbronorite sequences. Euhedral orthopyroxene primocrysts (Opx) contain tiny plagioclase inclusions, and are separated by small groundmass plagioclase laths. The plagioclase grains trapped between sutured orthopyroxene primocrysts should be noted. Field of view is 6 mm. (d) WBP UZ gabbronorite 56. Euhedral orthopyroxene primocrysts (Opx) contain tiny plagioclase inclusions, and are separated by similarly sized groundmass plagioclase with isolated, larger phenocrysts. The ragged, prismatic, post-cumulus clinopyroxene (Cpx) should be noted. Field of view is 6 mm.

The cellular-textured plagioclase domain is constituted of large, patchily zoned (An73·4–80·7) plagioclase grains that have scalloped edges and internal vein networks (Fig. 9b and d) filled with orthopyroxene (Opx Mg-number 66–67·4), Fe-rich clinopyroxene, pigeonite, ilmenite, quartz, alkali feldspar and mica. Vein pyroxenes may form optically continuous oikocrysts that extend into the hypidiomorphic host gabbronorite (Fig. 9b and d). Cellular-textured plagioclase is re-equilibrated to more evolved compositions (to An54·5–69·7) along vein edges (Fig. 9d), giving it a 'cellular' appearance reminiscent of a honeycomb, or of cells in a leaf. Cellular-textured plagioclase may contain gabbronoritic domains (An76·4–79·9) with textures and compositions similar to those of the host gabbronorite, suggesting that cellular-textured feldspar is a recrystallization or replacement product of the LMZ gabbronorite. Similar textures occur locally in MZ and UZ rocks (see below). The anorthosite domain (Fig. 9a and c) is dominated by neoblastic plagioclase (An73·1–82·2), with isolated laths (An77·3–80·3) and partly recrystallized micro-phenocrysts (An55·9–77·3). A discontinuous rind of granular pyroxene (Opx Mg-number 73·8–83) locally separates gabbronorite from anorthosite (Fig. 9a).

Lower Zone (LZ) websterite

Lower Zone websterite is dominated by sub-euhedral to euhedral, prismatic cumulus orthopyroxene primocrysts (*c.* 30–50%, 1–7 mm), which are embedded in a finer-grained, feldspar-rich groundmass (Figs 10a, b, and 11–14). Orthopyroxene primocrysts are normally zoned (Figs 11, 12 and 15), with core Mg-number and Cr_2O_3 contents similar to those of chilled margin micro-phenocrysts (Fig. 15). Many orthopyroxene primocrysts have serrated edges,

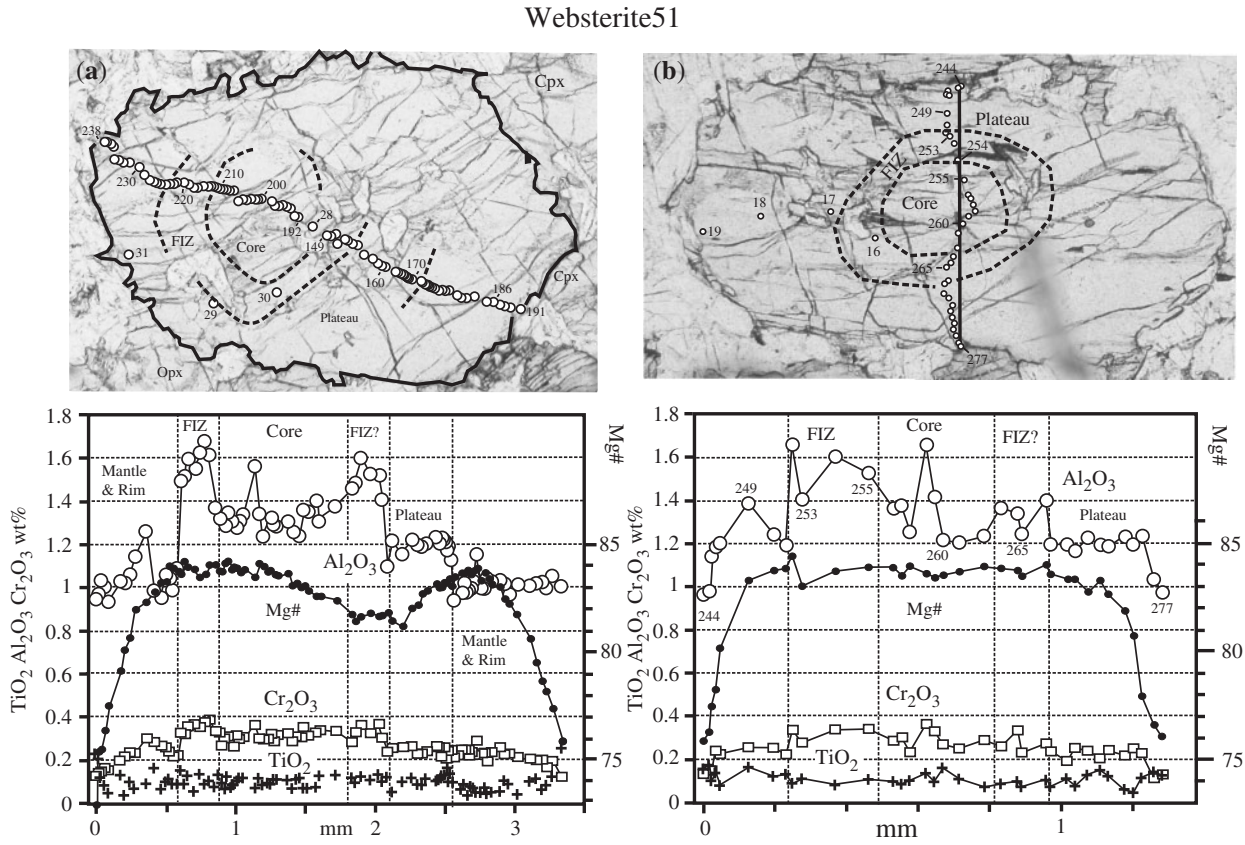

Fig. 11. (a and b). Electron microprobe traverses and corresponding photomicrographs across two orthopyroxene primocrysts in WBP LZ websterite 51. Numbers adjacent to spots are analysis numbers. FIZ, feldspar inclusion zone. The existence of anhedral, moderate Mg-number and moderately high Al_2O_3 (*c.* 1·3%) feldspar-free cores, surrounded by a higher-Al_2O_3 (*c.* 1·5%) zone (FIZ) where plagioclase inclusions appear, should be noted. The FIZ is surrounded by a laterally impersistent lower-Al_2O_3 (*c.* 1·2%) plateau. The phenocryst on the left shows a wide, low-Al_2O_3 (1%) normally zoned mantle, which is followed in both grains by a strongly zoned rim. The probe traverse in the grain on the right (b) does not show this low-Al_2O_3 (1%) mantle, presumably because of sector-zoning (see Fig. 12d). It should be noted that in both grains Cr_2O_3 decreases outward fairly systematically, whereas TiO_2 shows significant increases only in the outermost rim (see Fig. 12c).

with small Fe–Ti-rich protuberances that fill spaces between feldspar laths, and that probably represent epitaxial overgrowths on cumulus grains (e.g. Figs 10a and 12).

Orthopyroxene primocrysts commonly form a touching framework, with plagioclase laths sandwiched between the orthopyroxenes (Fig. 10a). Most orthopyroxene primocrysts contain sub-euhedral to ovoid inclusions of fine-grained plagioclase (Figs 10 and 11), suggesting coprecipitation of these phases over a significant interval. Feldspar inclusions can define concentric zones around anhedral, feldspar-free orthopyroxene cores, suggesting an early stage of orthopyroxene-only crystallization (e.g. sample 51, Fig. 11). In this example, the orthopyroxene zone where plagioclase inclusions first appear is enriched in Al_2O_3. Most plagioclase inclusions are tiny (*c.* 0·1–0·5 mm, Fig. 10a), but a few are larger (*c.* 1 mm, Fig. 10b). Rare, ovoid (0·1–0·5 mm) iddingsite inclusions show curved internal fractures typical of olivine. Orthopyroxene commonly shows faint sector-zoning (e.g. Fig. 12d). Primocrysts are commonly fractured, with fluid or melt inclusions surrounding the curved fractures (Fig. 10b), which may terminate against domains of intergranular biotite. This suggests fluid exsolution late in the crystallization history.

Plagioclase feldspar constitutes about 25–40% of the LZ websterite, and can be divided into four textural varieties (Figs 10a, b, 11 and 13): (1) 'phenocrystic' (>1 mm, <4 mm); (2) inclusions in orthopyroxene; (3) groundmass laths (c. 0·1–1 mm), which may be embedded in post-cumulus clinopyroxene; (4) intergranular to granophyric. We will argue that types 1–3 represents a single population of crystals that was injected together into the sill, and use the term 'phenocryst' simply to highlight the coarser size of some crystals. There is, in fact, a complete gradation from groundmass to phenocrystic plagioclase, and the

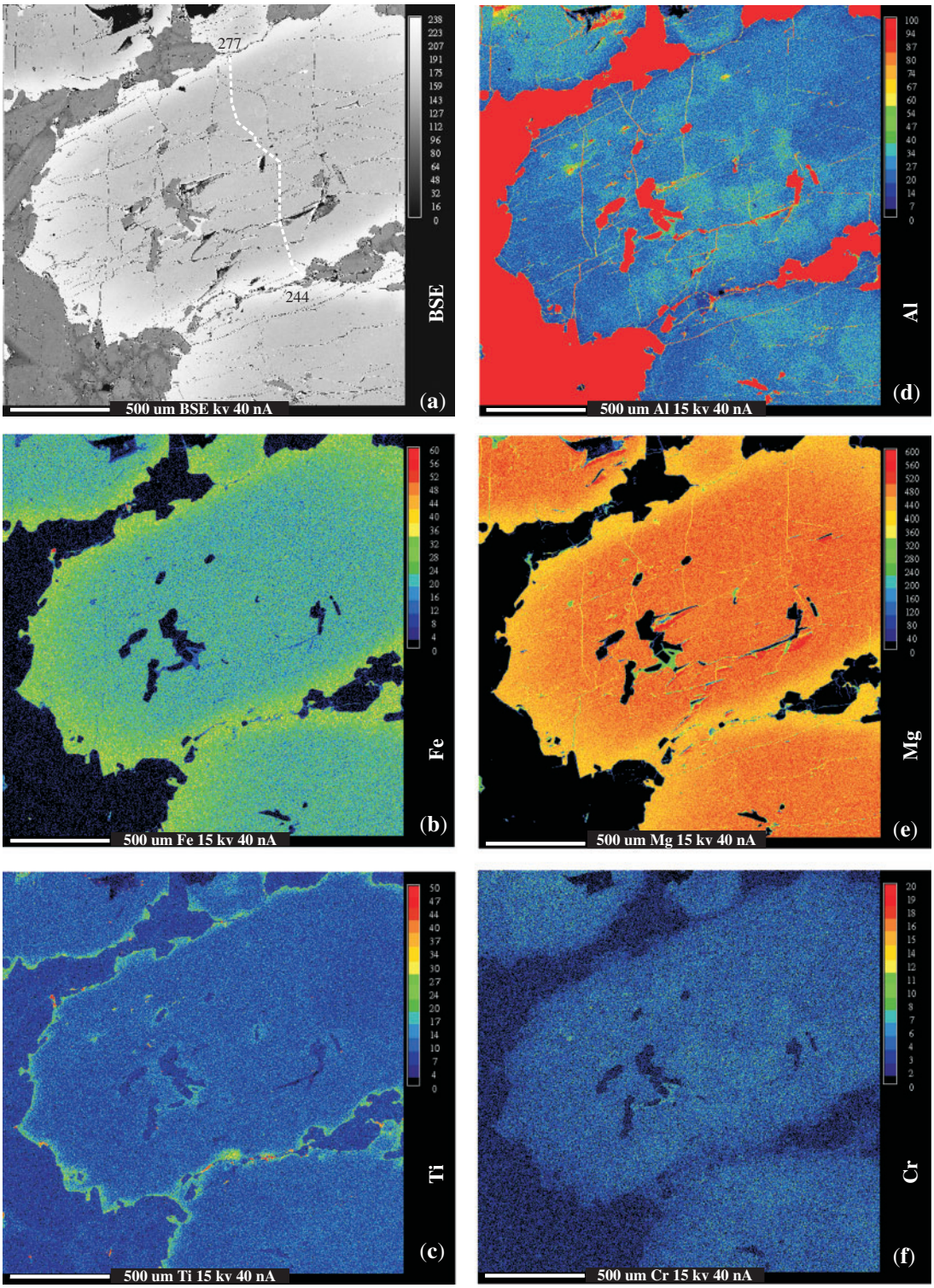

Fig. 12. Element maps of an orthopyroxene primocryst from WBP LZ websterite 51, corresponding to the right-hand image from Fig. 11b (inverted image). Element maps were made on a 2048 × 2048 micrometer area with a 512 × 512 pixel grid, with 20 ms count times/pixel at 15 kV and 20 nA. (a) Backscattered electron image showing probe traverse from Fig. 11b. (b) Fe, (c) Ti, (d) Al, (e) Mg, and (f) Cr concentration maps. The broad zone of concentric Mg depletion and Fe enrichment (b and e) is decoupled from the very narrow zone of Ti enrichment, which is restricted to the rim (c). Al is moderately enriched in the core, but decreases towards the tips, but not the sides, suggesting weakly developed sector-zoning (see Schwandt & McKay, 2006).

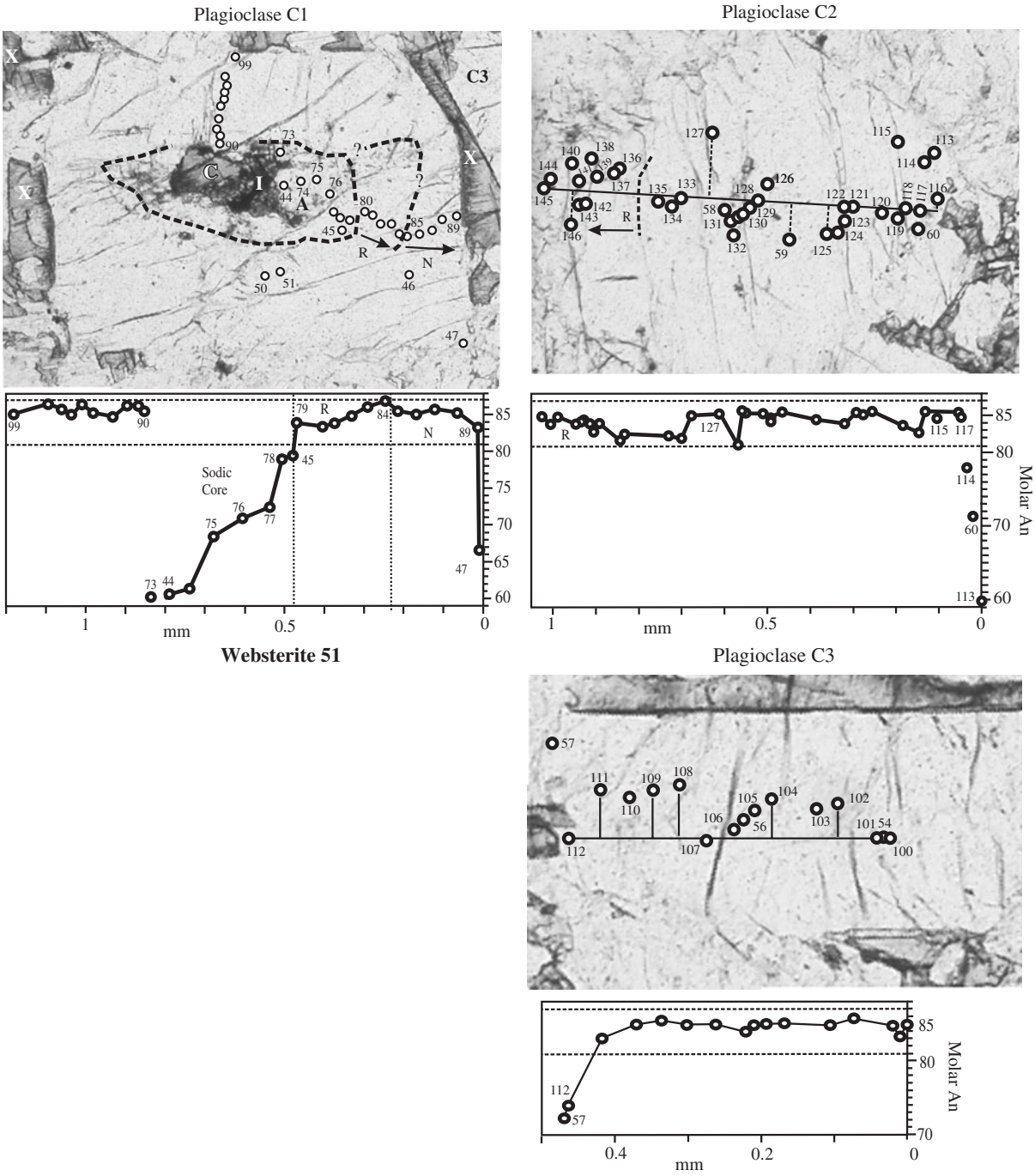

Fig. 13. Electron microprobe traverses across three plagioclase phenocrysts in WBP LZ websterite 51. Phenocryst C1: C, clinopyroxene inclusion; I, ilmenite inclusion; X, interstitial clinopyroxene; A, sodic plagioclase xenocrystic inner core; R, reversely zoned, xenocrystic(?) inner mantle; N, normally zoned outer mantle. Numbers adjacent to spots are analysis numbers. Phenocryst C1 is shown as element maps in Fig. 14. Phenocrysts C2 and C3 differ from C1 in having a broadly constant composition, with only a narrow outer sodic rim. Phenocryst C2 shows a narrow outer reversed zone (R).

distinction is purely descriptive. Most euhedral plagioclase phenocrysts are rather uniform in composition, with only minor normal zoning near the edges (Fig. 13, grains C2 and C3). However, some contain complexly zoned anhedral cores that are more sodic than the enveloping mantle (Figs 10b, 13 and 14), and that are associated with quartz, orthoclase, ilmenite, biotite, and clinopyroxene (Figs 10b and 13). Small plagioclase laths embedded in

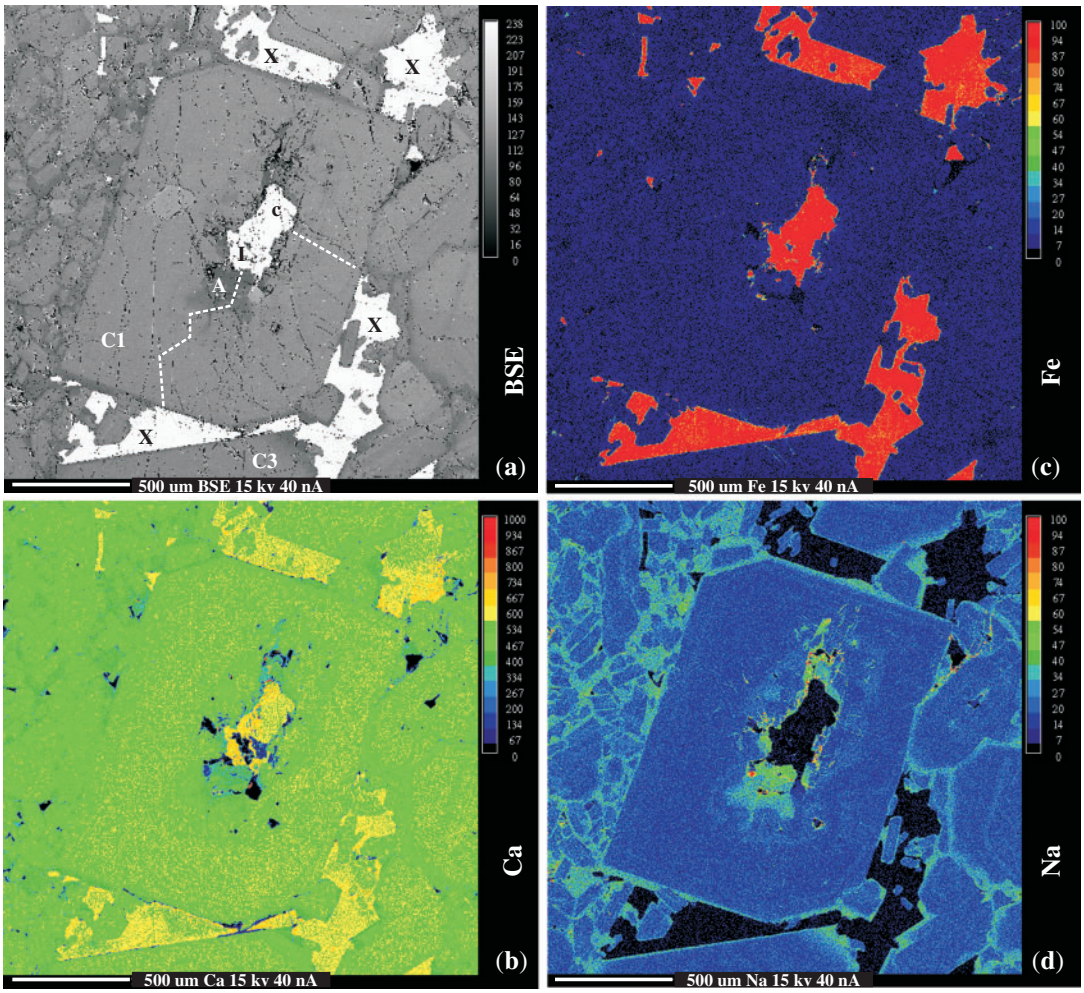

Fig. 14. Plagioclase phenocryst C1 from WBP LZ websterite 51. (See Fig. 12 for details of analysis.) (a) Backscattered electron microprobe image with path of traverse from Fig. 13 shown. (b) Ca, (c) Fe and (d) Na concentration maps. Noteworthy features are the irregular, anhedral sodic plagioclase core (A); the extremely narrow outer sodic rim, suggesting minimal re-equilibration with interstitial evolved melt; and the complex mesh of Na-enriched plagioclase in the groundmass to the left. C, clinopyroxene inclusion; I, ilmenite inclusion; X, interstitial clinopyroxene; A, sodic plagioclase inner core.

orthopyroxene tend to be rounded, rarely showing facets. Most plagioclase occurs as small, sub-euhedral, normally zoned, 'groundmass' laths (Fig. 10a), typically sandwiched between sutured orthopyroxene primocrysts. Some of the plagioclase grains trapped between adjoining orthopyroxene phenocrysts are bent (see below, Fig. 18b), indicating that significant force was exerted by the compacting orthopyroxene primocrysts, and that feldspar was mechanically trapped and deformed by this process. In some cases, these inter-granular sites are larger, forming distinct feldspar-rich 'pools' or patches, with randomly oriented plagioclase laths and abundant interstitial granophyre. Intergranular very fine-grained anhedral plagioclase is subordinate, more sodic (Fig. 16), and is commonly intergrown with quartz. The compositions of groundmass laths overlap the range of phenocryst plagioclase and of plagioclase inclusions in orthopyroxene (Fig. 16a).

Clinopyroxene (10–30%, 0·1–7 mm, average *c.* 1 mm) is typically interstitial, ophitic or oikocrystic (Figs 9a and 13), and appears to replace orthopyroxene (Fig. 10a). Inclusions of plagioclase are common. Clinopyroxene may have ragged prismatic to acicular forms, but true 'cumulus' grains are not observed. Interstitial sites are commonly occupied by quartz, alkali feldspar, ilmenite, rutile, and biotite. Ilmenite is the dominant Fe–Ti-oxide, with minor magnetite exsolution and/or rutile intergrowths. Interstitial sulphide is extremely rare.

Lower Zone (LZ) feldspar-rich rocks

The LZ contains three types of feldspar-rich rocks: (1) centimeter-scale anorthositic schlieren and veinlets (Figs 5a, b and 6); (2) centimeter- to decimeter-scale leuco-gabbronoritic 'veins' (Fig. 5d) and meter-scale 'pipes' (Fig. 6); (3) meter- to decameter-scale layered

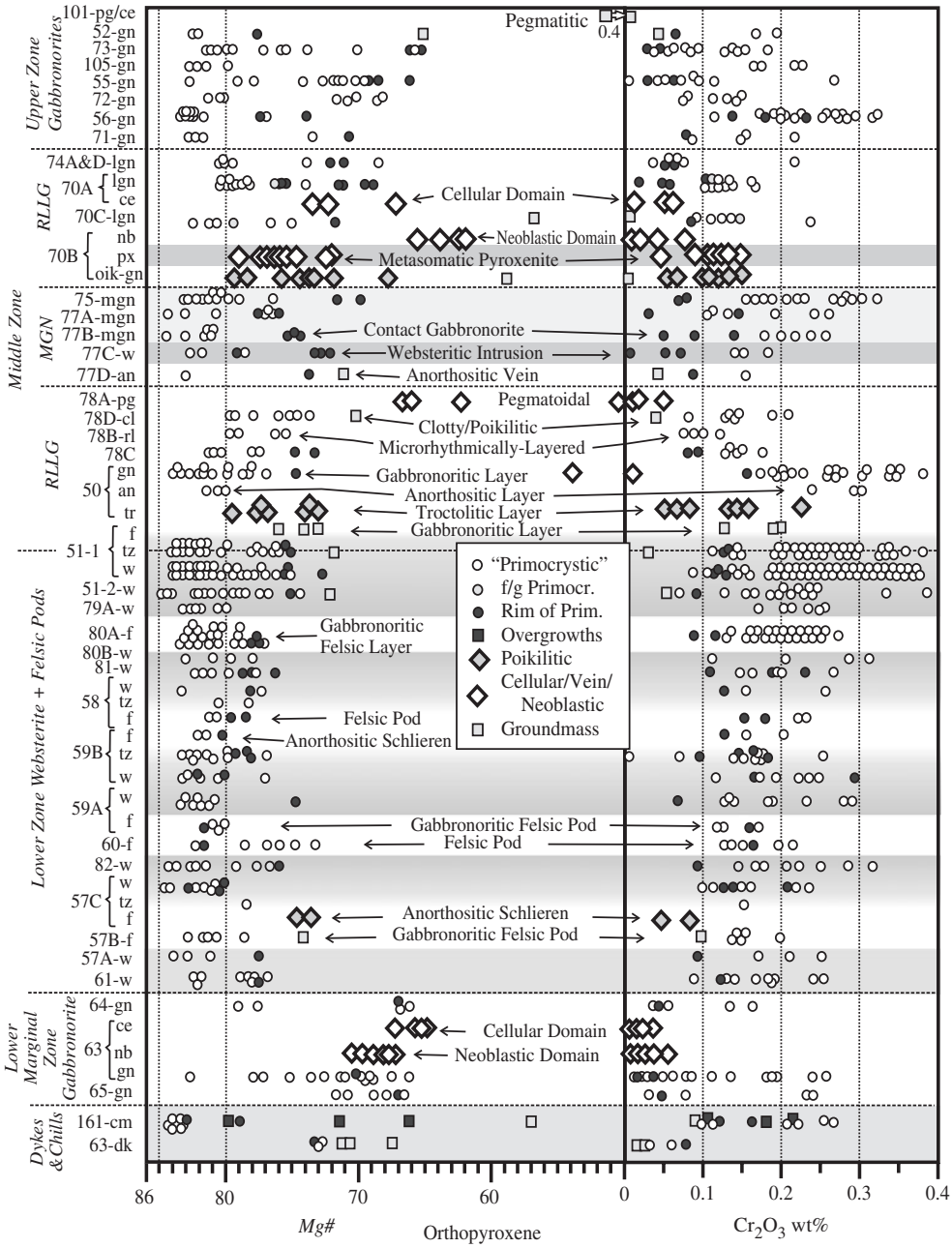

Fig. 15. Pseudo-stratigraphic column showing orthopyroxene compositional variations. Mg-number = $100 \times Mg/(Mg + Fe^{total})$. Samples from both sections (Dais and WBP) have been merged in the correct stratigraphic order, although absolute stratigraphic heights are not respected (see Fig. 4). Grey shading in LZ, MZ and UZ reflects lithology (dark grey, pyroxenite; pale grey, transition to felsic rocks; white, gabbroic). Analyses are classified according to texture. Sample numbers (e.g. sample 72-gn) have suffixes as follows: dk, dyke; cm, chilled margin; gn, gabbronorite; lgn, leuco-gabbronorite; mgn, mela-gabbronorite; nb, neoblastic; ce, cellular-textured; w, websterite; f, felsic pod; tz, transition zone between host websterite and felsic pod; an, anorthositic; oik, oikocrystic; px, pyroxenitic; tr, troctolitic; pg, pegmatoidal; FeG, ferrogabbro; cl, clotty-poikilitic; rl, microrhythmically layered; LGN, leuco-gabbronorite; MGN, mela-gabbronorite; RLLG, rhythmically layered leuco-gabbronorite sequences. The virtual absence of cryptic variation of orthopyroxene primocryst compositions should be noted.

leuco-gabbronorite sequences straddling the transition from the LZ to the UZ (Figs 3 and 7a). The last are described with the MZ rocks and are best developed in the Dais Intrusion (Figs 3 and 4).

Anorthositic schlieren

Anorthosite occurs as spaced rhythmic bands (some branching), as interconnected branching vein networks, or as irregular veinlets peripheral to larger felsic pods

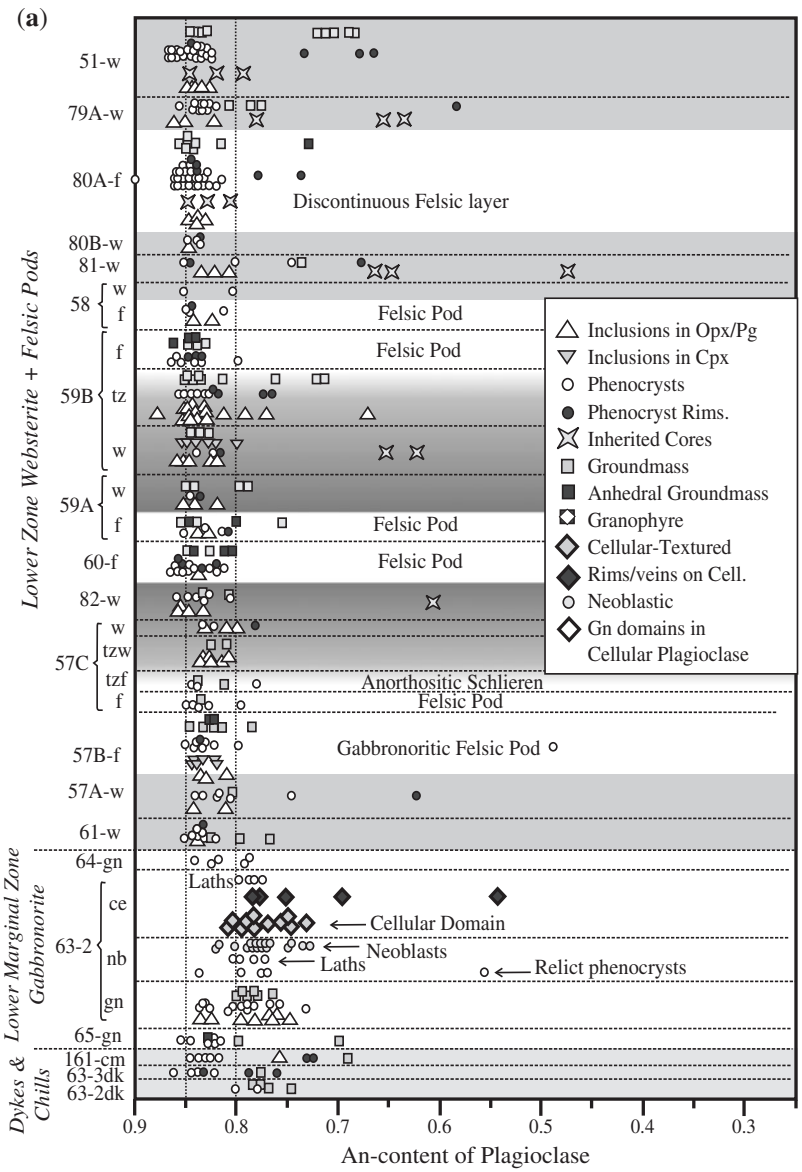

Fig. 16. Pseudo-stratigraphic column showing plagioclase compositional variations (molar anorthite content) from base (a) to top (c). Suffixes and other notes as in Fig. 15. The virtual absence of cryptic variation of compositions among and between phenocrysts, inclusions and groundmass laths should be noted.

(Figs 5a-c and 6). There are no obvious textural or mineral-chemical differences between these three parageneses, all of which are dominated by fine-grained plagioclase laths, with subordinate (10–15%) feldspar phenocrysts (>1 mm) and rare euhedral orthopyroxene primocrysts (see below, Fig. 18b and c); and all will be referred to as 'anothositic schlieren' henceforth. Typically, feldspar laths (0·2–0·5 mm) are aligned parallel to veinlet or schlieren contacts. Shapes, grain sizes, zoning patterns and compositions of feldspars are identical to what is seen in the adjoining websterites (Fig. 16a and b), with no systematic compositional difference between phenocrystic, inclusion and groundmass feldspar. Anhedral intergranular plagioclase and minor quartz (± clinopyroxene, alkali feldspar and ilmenite) cement the laths. Rare, euhedral orthopyroxene primocrysts (with plagioclase inclusions) float within the feldspar-rich matrix, and have textures and compositions identical to those of orthopyroxene primocrysts from the adjoining websterites (Fig. 15). Ca-rich clinopyroxene is invariably interstitial or poikilitic, and shows no systematic compositional differences in comparison with clinopyroxene from the host websterites (Fig. 17). To summarize, the textures

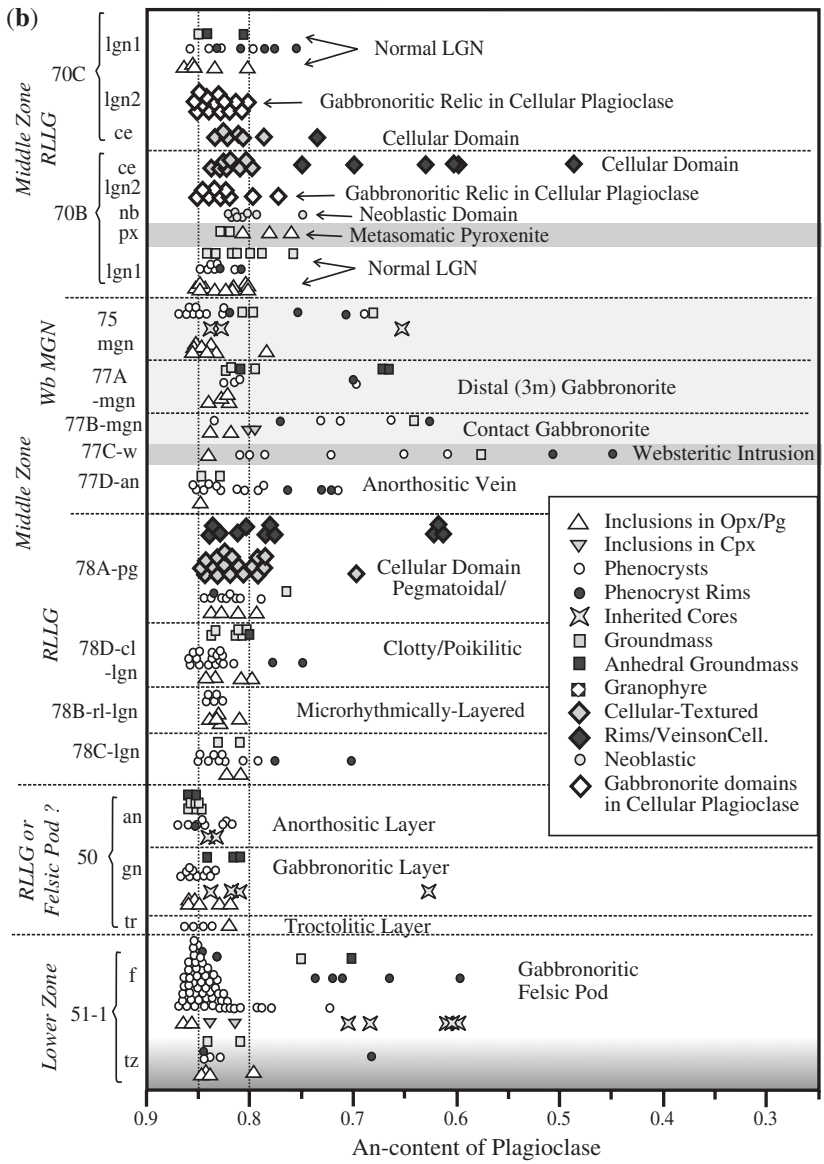

Fig. 16. Continued.

in these anorthositic schlieren are essentially identical to the feldspar-rich intercumulus matrix in the websterites.

Gabbronoritic to anorthositic veins and pipes

Larger feldspar-rich bodies in the LZ tend to be zoned, with anorthositic margins and gabbronoritic cores (Figs 5d, 6 and 18). The anorthositic margins are texturally identical to the schlieren described above, with similar mineral-compositional ranges (Figs 15–17) and textures (Fig. 19b). The feldspar foliation in the pod margin anorthosite may truncate (erode?) the foliation of the parasitic anorthositic veinlets or schlieren. The cores of the felsic pods are composed of gabbronorite and leuco-gabbronorite with very similar textures (Fig. 18a and d). Orthopyroxene primocrysts are sub-euhedral (Fig. 19a), and are only slightly more evolved than typical websterite orthopyroxenes (Fig. 15), a difference that can easily be accounted for by the effect of the trapped liquid shift acting on a rock with a smaller pyroxene mode (see Barnes, 1986; Chalokwu & Grant, 1987; Cawthorn *et al.*, 1992). Fe–Ti-rich epitaxial pyroxene overgrowths fill spaces between feldspar laths. Clinopyroxene is interstitial, ophitic, poikilitic, or occurs as long (up to 10 cm), curved, ragged blades that grow across the feldspar foliation (Fig. 18a), and that show no sign of internal strain. This implies that the crystallization of clinopyroxene

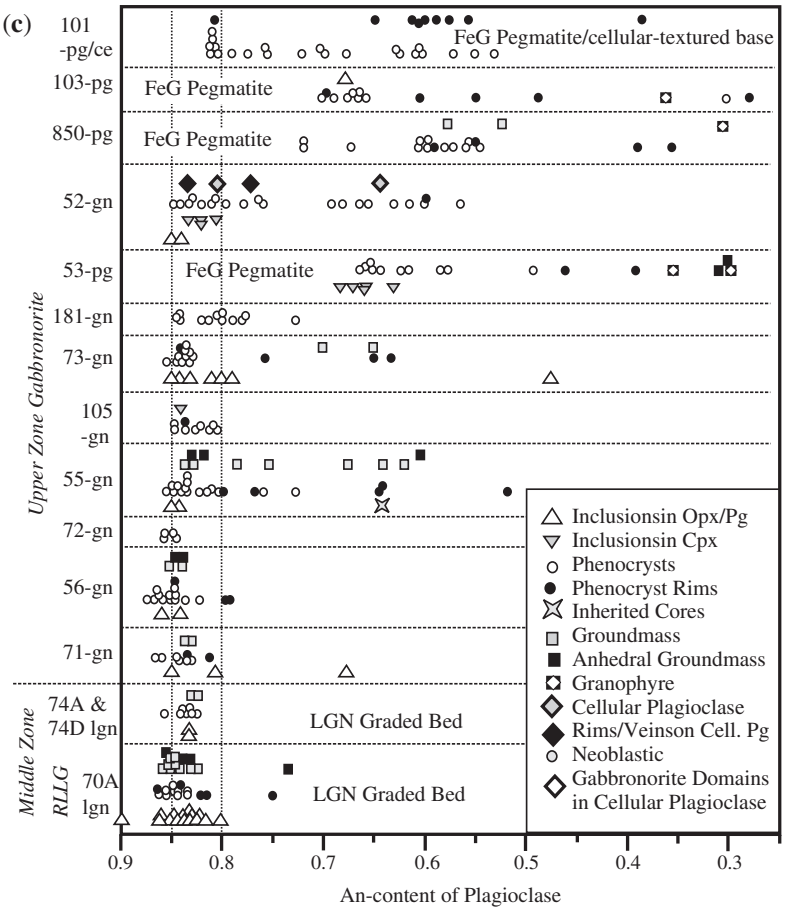

Fig. 16. Continued.

post-dates development of the feldspar flow foliation. Clinopyroxene is only slightly more evolved than in the websterites (Fig. 17), possibly also reflecting the trapped liquid effect.

One feldspathic 'layer' in the uppermost LZ at WBP is notable for the presence of fresh olivine (Fig. 20a, Fo 74·8–70·3, 0·5–1 mm) in an anorthositic olivine gabbronorite band (*c.* 1 cm thick, sample 50-tr) that is texturally and compositionally similar to the anorthositic schlieren described above. Gabbronorite that is interlayered with the anorthosite contains large (<7 mm), sub-euhedral orthopyroxene primocrysts that are partly replaced by coarse (<8 mm) poikilitic clinopyroxene (Fig. 20b). The textures could be interpreted to suggest that the clinopyroxene component was expelled from the anorthositic layers, to crystallize in the intervening gabbronoritic layers.

Middle Zone (MZ)

As discussed above, a formal Middle Zone cannot be distinguised in the WBP area. In the Dais Intrusion, the MZ is characterized by two prominent contact-parallel sequences of rhythmically layered leuco-gabbronorite (Figs 3, 4 and 7a), separated by mela-gabbronorite.

The mela-gabbronorite

The mela-gabbronorite of the MZ is texturally and mineralogically (Figs 7b and 10c, samples 75, 77A and 77B) very similar to typical LZ websterite and UZ porphyritic gabbronorite, and appears to represent a gradational transition between these two facies. In terms of mineral chemistry (Figs 15–17) it shows the same compositional and textural systematics as these two facies.

Websteritic intrusion

A 2 m × 1 m websterite body (Fig. 7b: sample 77C) was emplaced into MZ mela-gabbronorite in the Dais MZ. The intrusive websterite is texturally and mineralogically very similar to the LZ feldspathic websterites (Figs 15 and 16b), except for the presence of more evolved (An51–81: Fig. 16b), coarser, anhedral to lath-shaped plagioclase in the groundmass. The groundmass of this sample also contains an unusually large proportion of brown–red mica, ilmenite + rutile and cuneiform quartz + plagioclase

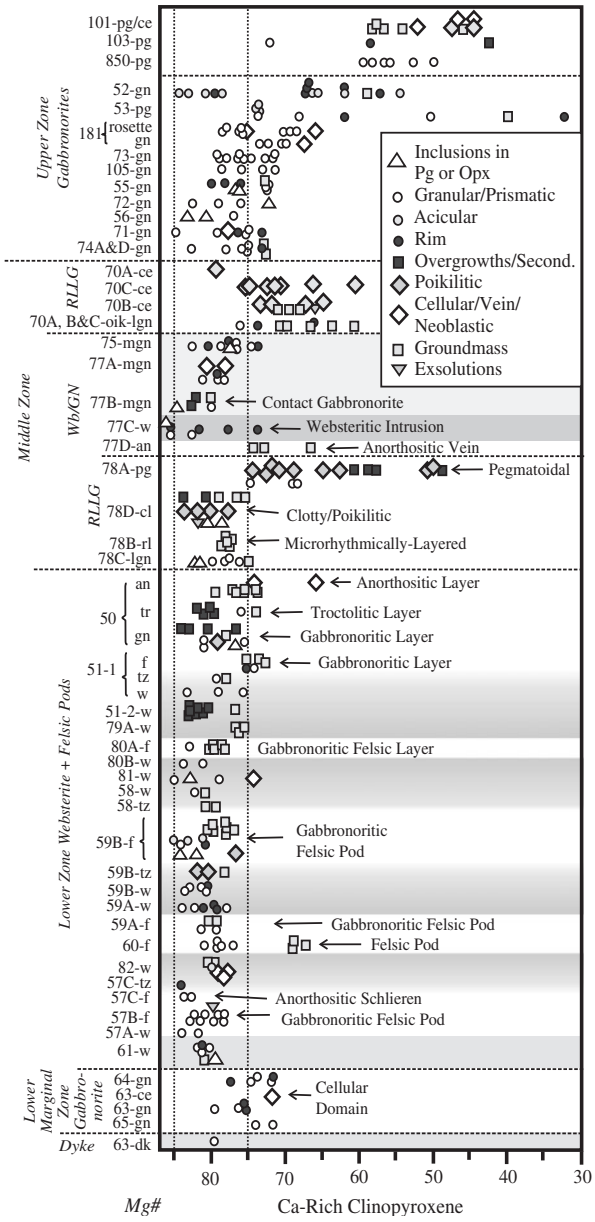

Fig. 17. Pseudo-stratigraphic column showing Ca-rich clinopyroxene compositional variations (Mg-number = $100 \times Mg/Mg + Fe^{total}$) from base to top. Suffixes and conventions as in Fig. 15.

(An21) + orthoclase (Or71–79) intergrowths. An anorthositic vein (sample 77D) occurs at one contact of this websterite intrusion (Fig. 7b). It is similar in texture and composition to the anorthositic schlieren and pod margins from the LZ (described above).

The rhythmically layered leuco-gabbronorite sequences of the Dais Intrusion

The rhythmically layered leuco-gabbronorite sequences are extremely complex. The most common facies is a gabbronorite to leuco-gabbronorite (Figs 7a and 21a, b) that closely resembles the facies found in the feldspar-enriched pods and schlieren that occur within LZ websterite (see above), and that is texturally very similar to UZ porphyritic-textured gabbronorite (Fig. 10d; see below). The MZ gabbronorites and leuco-gabbronorites from the layered sequences are foliated parallel to layering and commonly show inward coarsening from both upper and lower contacts. Orthopyroxene primocrysts coarsen inward from <1 mm to a maximum of about 8 mm, and are commonly stuffed with plagioclase inclusions (Fig. 21a). Orthopyroxene is slightly more evolved than in the LZ or UZ (Mg-number <81, Fig. 15), presumably as a result of the trapped melt effect and a low pyroxene mode. Most orthopyroxene primocrysts have wide, Fe-enriched overgrowths that extend into the spaces between feldspar laths, giving them the appearance of oikocrysts (Fig. 21a). Epitaxial overgrowths are composed of Fe-enriched orthopyroxene (Fig. 15), clinopyroxene (Fig. 17), or Fe-rich pigeonite (some inverted). In one well-characterized sample (70B), Fe-rich clinopyroxene overgrowths are restricted to the sides of an orthopyroxene primocryst (Fig. 21a and b), suggesting post-cumulus growth in a strain-shadow during compaction. Feldspars have textures and compositional ranges similar to those of LZ websterites and UZ gabbronorites (Fig. 16), with near-complete overlap between the compositional range of the different feldspar parageneses (inclusions in orthopyroxene An <90, phenocrystic plagioclase An <87, groundmass laths An <86, Fig. 16). Clinopyroxene (Mg-number 70·2–82·9) forms oikocrysts, and minor interstitial biotite, quartz, ilmenite, magnetite and pyrite rimmed by magnetite are observed.

As discussed above, the contacts between leuco-gabbronorite layers are locally decorated by stringers of pyroxenite + coarse plagioclase (Fig. 7a), which may extend along-strike to form thicker discordant bodies (Fig. 7d). One of these contact zones was examined in detail (Figs 21c, d and 22, samples 70A, B and C), providing constraints on the relative timing of melt segregation, cooling, deformation and recrystallization. The lower leuco-gabbronorite layer (sample 70B-lgn1) grades up into a 3–5 mm thick poikilitic pyroxene-rich gabbronorite ('PP' in Fig. 21c) with Fe-rich orthopyroxene (Mg-number <80, sample 70B-oik-gn, Fig. 15). This pyroxene-rich gabbronorite grades up into a thin (1 mm), laterally discontinuous, granular- or mosaic-textured, orthopyroxene-rich, feldspar-poor websterite ('GP' in Fig. 21c), also with Fe-rich orthopyroxene (Mg-number <80, sample 70B-px, Fig. 15), whereas plagioclase is slightly less calcic than usual (An <83: sample 70B-px, Fig. 16b). The textures and compositions suggest that the pyroxene grew late. There follows a thin (1 mm), laterally discontinous anorthositic neoblastic zone (An <83, sample 70B 'nb' in Fig. 16, 'n' in

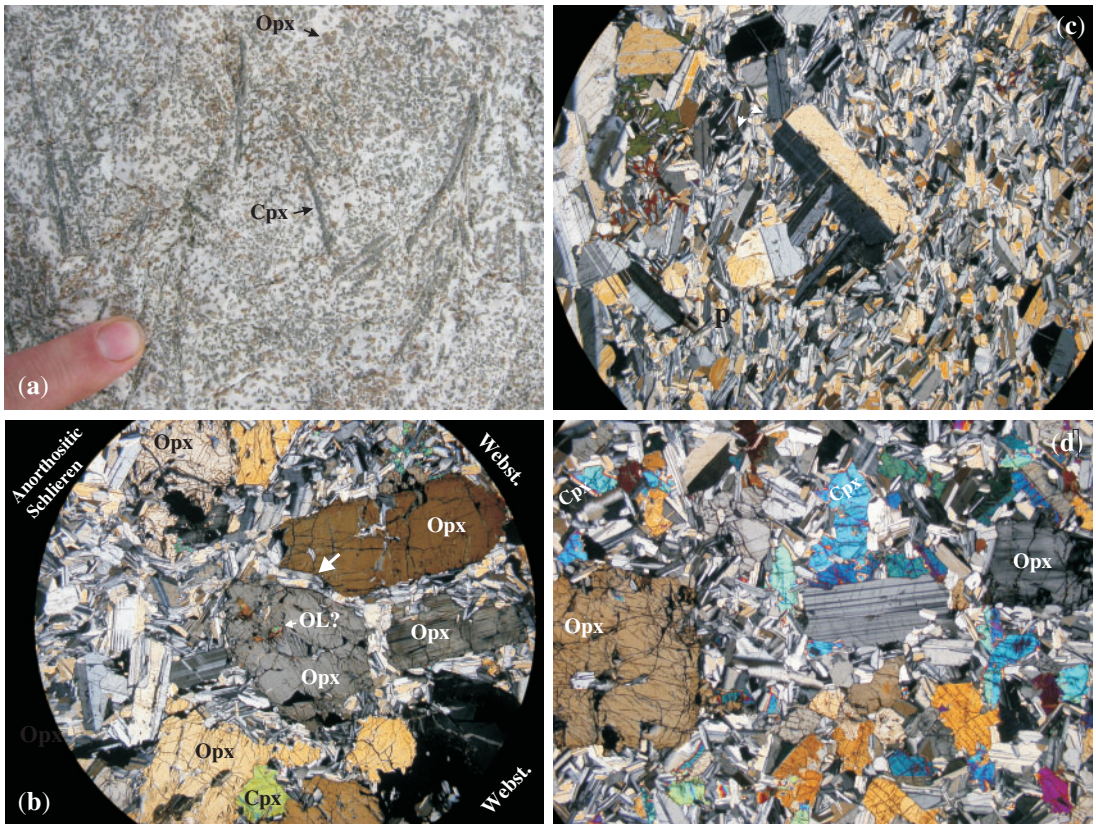

Fig. 18. (a) Field photograph of jackstraw-textured core of felsic pipe 57B from the WBP LZ (*c.* 1 m wide, see Fig. 6a). The acicular clinopyroxenes, and more prismatic orthopyroxenes, should be noted. (b) WBP LZ sample 59B (see Fig. 6b), showing transition from host websterite to anorthositic schlieren. Noteworthy features are the closely packed orthopyroxene primocrysts (Opx) in the host, with common feldspar inclusions and rare, ovoid pseudomorphs after olivine (OL?) inclusions; the interstitial-textured clinopyroxene (Cpx); the tendency for groundmass plagioclase to be aligned parallel to orthopyroxene faces and apparently feeding towards the anorthositic schlieren; and the fact that plagioclase trapped between orthopyroxene phenocrysts is bent (arrow), suggesting mechanical compaction. In contrast to the websterite, the foliation in the anorthositic schlieren parallels the contact, with a concentration of larger phenocrysts plated against the websterite. Field of view is 7 mm; crossed Nicols. (c) WBP LZ anorthositic schlieren feeding a larger felsic pod (sample 57C), showing presence of coarser plagioclase phenocrysts in a foliated anorthositic matrix. Field of view is 7 mm; crossed Nicols. (d) WBP LZ core of felsic pod (sample 59A), showing euhedral orthopyroxene (Opx) primocrysts, plagioclase phenocrysts (albite twinned), abundant foliated groundmass plagioclase, and interstitial clinopyroxene (Cpx). Field of view is 6 mm; crossed Nicols.

Figs 21c, d and 22a), which implies recrystallization of feldspar during deformation. Pyroxene from the GP layer overgrows the feldspar neoblasts (Fig. 21d), indicating that pyroxene growth post-dates deformation recorded in the anorthositic neoblastic zone. Taken in tandem with the observation that Fe-rich clinopyroxene occupies strain-shadows in the compacting leuco-gabbronorite (Fig. 21a and b), it seems reasonable to infer that the melt from which the pyroxene grew was expelled from the compacting leuco-gabbronorite and was concentrated at the contact (Fig. 7a).

The anorthositic neoblastic zone grades rapidly up into a thin, laterally discontinuous gabbronoritic layer (Fig. 21c and 22a, 1 mm thick), which looks like 'normal' leuco-gabbronorite, and has feldspars of similar composition (sample 70B-lgn2, Fig. 16b). This 'normal' gabbronorite grades into a 1–2 cm thick 'cellular-textured' plagioclase domain (Fig. 22) characterized by large (5–10 mm) grains with compositionally homogeneous cores that are only slightly less calcic than usual (An <84·7, sample 70B-ce, Fig. 16b), and that may show faint, irregular, patchy zoning. The cellular-textured plagioclase may completely envelop patches of gabbronorite that are indistinguishable from normal, background gabbronorite and leuco-gabbronorite (sample 70B-lgn2, Fig. 16b). The existence of such relict gabbronoritic patches suggests that cellular-textured plagioclase developed at the expense of the host gabbronorite through some type of recrystallization–replacement process. Cellular-textured plagioclase grains have scalloped edges and are surrounded and veined by assemblages of (in order of abundance) clinopyroxene, quartz, alkali feldspar, ilmenite (± magnetite exsolution), pigeonite, orthopyroxene, biotite, and hornblende (Fig. 22).

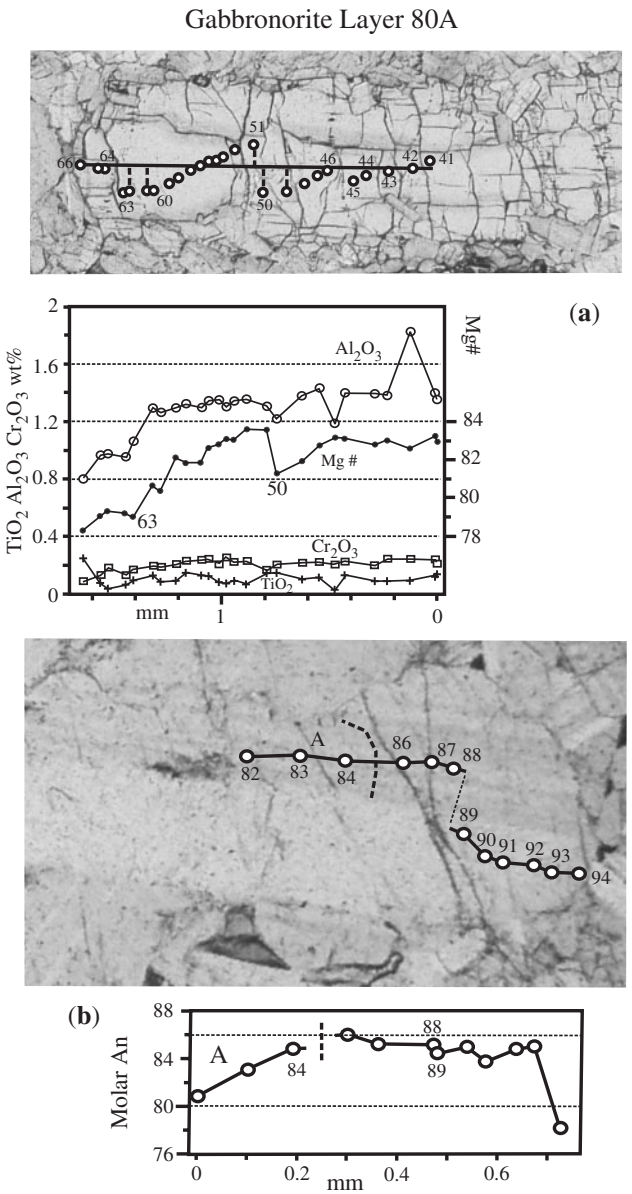

Fig. 19. Dais LZ gabbronorite layer sample 80A in websterite. (a) Electron microprobe traverse and corresponding photomicrograph across an orthopyroxene primocryst. Numbers adjacent to spots are analysis numbers. This example shows a fairly systematic outward decrease in Mg-number (with a few kinks), Al_2O_3 and Cr_2O_3. In contrast, TiO_2 shows significant increases only in the outermost rim. (b) Microprobe traverse and corresponding photomicrograph across a plagioclase phenocryst. A, sodic plagioclase inherited(?) core. The near-constant high-An mantle and narrow sodic rim should be noted.

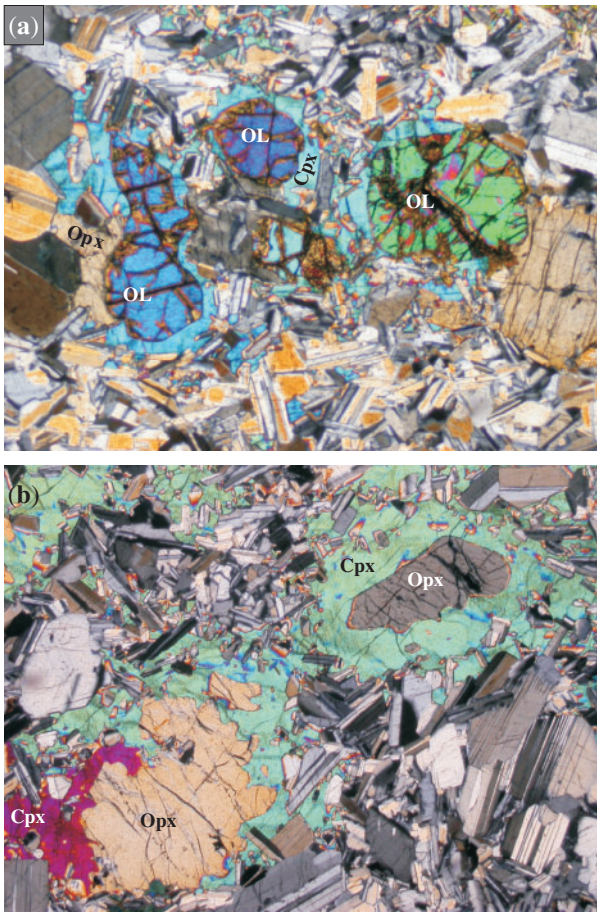

Fig. 20. WBP LZ leucocratic layer 50. Crossed Nicols. (a) Anorthositic noritic troctolite layer. The ovoid, partly resorbed olivines (OL) with orthopyroxene (Opx) and clinopyroxene (Cpx) rims should be noted. Plagioclase (twinned grains) show a preferential east–west alignment, parallel to layering. Field of view is 3·5 mm. (b) Gabbronoritic layer sandwiched between two anorthositic layers. The large clinopyroxene (Cpx) oikocrysts enveloping plagioclase and replacing orthopyroxene (Opx) should be noted. Field of view is 7 mm.

Pyroxenes in different veins are typically in optical continuity on a centimeter scale (Fig. 22a and b), forming large 'oikocrysts' with no sign of internal strain, and are systematically more evolved than pyroxenes from the background gabbronorite or leuco-gabbronorite (sample 70A-ce in Fig. 15, samples 70A-B and C-ce in Fig. 17). The cellular-textured plagioclase is commonly re-equilibrated to more sodic compositions in a millimeter-scale halo around the veins and injections (Figs 16b and 22c, d). In places, twins and grain boundaries of the cellular plagioclase are offset, bent and rotated along sets of fractures now occupied by undeformed minerals of the evolved vein assemblage (Fig. 22b). This implies that the cellular-textured plagioclase was cold enough to fracture at the time the evolved melt from which the vein assemblage crystallized was injected. This further suggests that there may be a link between deformation (neoblasts, fractures) and movement of this evolved melt. The top of the cellular-textured plagioclase domain abuts directly against the base of the overlying, 2 m thick, reverse size-graded layer of foliated leuco-gabbronorite (sample 70A-lgn1 Fig. 16c, mostly An <86·6; Fig. 15 Opx Mg-number <81). The contact is

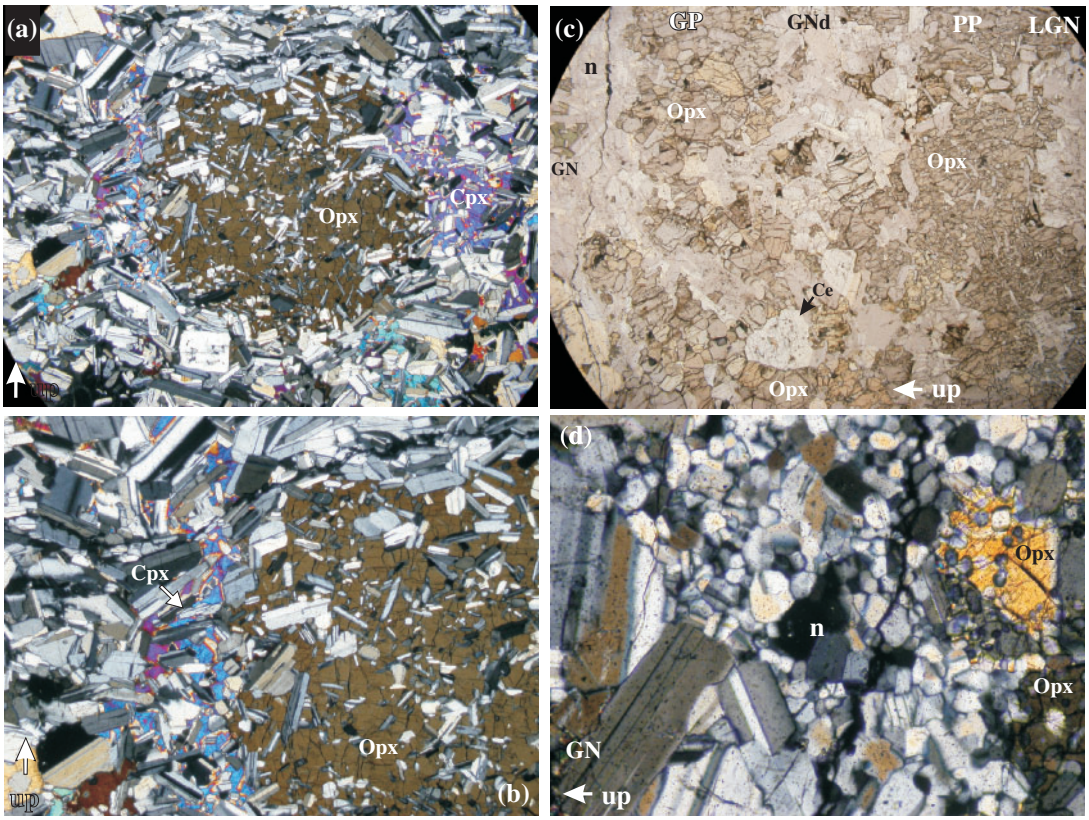

Fig. 21. Dais MZ rhythmically layered leuco-gabbronorite sequence showing the contact zone (sample 70B, see Fig. 7a) between two layers. Arrows show way-up. (a) Upper part of a 2 m thick leuco-gabbronorite layer. The orthopyroxene (Opx) oikocryst contains abundant, very fine-grained, randomly oriented, plagioclase laths, and is interpreted to represent a primocryst with adcumulus overgrowths. It should be noted that the plagioclase outside the oikocryst is coarser, and wraps around it. Clinopyroxene (Cpx) is concentrated in the pressure shadow to either side of the orthopyroxene oikocryst, suggesting that compaction expelled much of the melt from which clinopyroxene crystallized. The euhedral, zoned plagioclase 'phenocryst' in the bottom center of the image should be noted. Field of view is 7 mm. Crossed Nicols. (b) Close-up of (a) showing the clinopyroxene in the pressure shadow. Field of view is 4 mm. (c) Transition from the leuco-gabbronorite to the right (LGN, Fig. 21a), through a pyroxene-poikilitic zone (PP), a granular pyroxenitic zone (GP), a neoblastic zone (n), and then a narrow gabbronoritic zone (GN) transitional into the cellular plagioclase domain (Fig. 22). A discontinuous patch of relict(?) gabbronorite (GNd) is sandwiched between the poikilitic (PP) and granular pyroxenites (GP). A small, cellular-textured plagioclase grain (Ce) is embedded within the granular pyroxenite. Way-up is to the left. Field of view is 6·5 mm. Slightly crossed Nicols. (d) Sample 70B Close up of the neoblastic zone (n), showing how orthopyroxene (Opx) from the granular pyroxenite overgrows neoblastic plagioclase and so must post-date deformation. The neoblastic facies grades into gabbronorite (GN) and then into the cellular plagioclase facies further towards the left. Field of view is 1·2 mm. Crossed Nicols.

extremely irregular, and fragments (2 mm) of the cellular-textured plagioclase occur in the adjoining foliated leuco-gabbronorite layer, suggesting that they were detached and entrained into the overlying leuco-gabbronorite 'flow'.

A discordant body of pyroxene-enriched, 'pegmatoidal' leuco-gabbronorite (sample 70C) is located a meter along the extension of the contact (sample 70A-B) described above, and is composed of the same material as the cellular-textured plagioclase domain of sample 70B, with abundant poikilitic Fe-rich pyroxene, quartz and ilmenite, and all the other features that we suggest are associated with movement and impregnation by evolved melt (Figs 15, 16 and 23a). Pegmatoid sample 78A (Fig. 7d) is almost completely detached from its root zone, has evolved orthopyroxene (Mg-number <68, Fig. 15), two generations of Fe-rich clinopyroxene (Fig. 23b), and plagioclase compositions similar to those of the cellular-textured plagioclase from samples 70B and 70C (Fig. 16b).

Upper Zone (UZ) and Upper Marginal Zone (UMZ)

Gabbronorite textures in the Upper Zone range from porphyritic (Fig. 10d) to hypidiomorphic (Fig. 14), in some cases within a single thin section. There is also localized development of ferrogabbroic pegmatoids and rocks with incipient cellular textured plagioclase (Fig. 7c). UZ gabbronorites become finer-grained towards the upper contact of the sill (UMZ), and are essentially indistinguishable from LMZ gabbronorites.

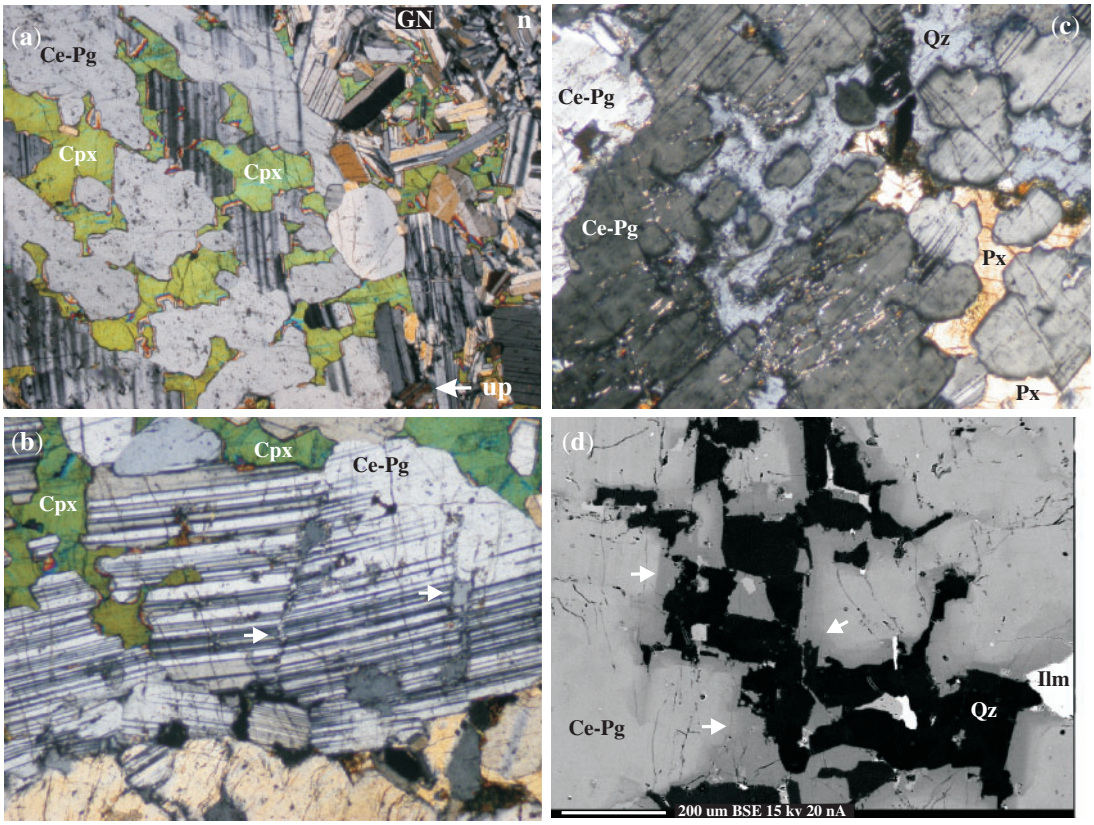

Fig. 22. Dais MZ rhythmically layered leuco-gabbronorite sequence showing the contact zone (sample 70B) between layers. (a) The neoblastic (n) and gabbronoritic (GN) zones of Fig. 21c and d give way to a cellular-textured plagioclase domain (Ce-Pg). The coarse grain-size, and scalloped shape of the plagioclase (pale grey and twinned), should be noted. Clinopyroxene (Cpx) forms centimeter-scale oikocrysts veining the cellular plagioclase. All of the Cpx in the field of view is in optical continuity. Field of view is 4 mm; crossed Nicols. Arrow shows way-up. (b) Cellular-textured plagioclase (Ce-Pg) veined by clinopyroxene (Cpx) oikocryst. It should be noted that the clinopyroxene is injected into what appears to be one of a set of fractures that offset and bend twin lamellae in the cellular-textured plagioclase, and also control the location of veins containing quartz, alkali feldspar, mica and ilmenite (arrows). Field of view is 2·8 mm; crossed Nicols. (c) Cellular-textured plagioclase (Ce-Pg) veined by pyroxene (Px), quartz (Qz), alkali feldspar, mica and ilmenite. The dark (sodic) rims around the cellular-plagioclase that are in contact with the vein assemblage should be noted. Field of view is 2·3 mm; crossed Nicols. (d) Electron microprobe backscatter image showing another example of a quartz-rich (Qz, black) impregnation–vein assemblage. Bright areas are ilmenite (Ilm). Arrows show the dark sodic rims to the cellular-plagioclase (Ce-Pg) that is in contact with the veins.

Porphyritic facies

Texturally, UZ porphyritic gabbronorite (Fig. 10d) is nearly identical to LZ websterite (Fig. 10a) and MZ mela-gabbronorite (Fig. 10c). Specifically: (1) sub-euhedral orthopyroxene primocrysts show the same zonation pattern and compositions, and commonly contain plagioclase inclusions (Figs 10d, 15, 26 and 27); (2) plagioclase has the same parageneses (phenocrysts, inclusions in orthopyroxene, groundmass laths, granophyre; Fig. 10d) and compositional ranges (Fig. 16); (3) plagioclase phenocrysts (Fig. 25) may have sodic cores (Fig. 16b and c); (4) clinopyroxene is generally post-cumulus (Fig. 10d); (5) groundmass assemblages are similar (ilmenite ± rutile ± magnetite intergrowths, and interstitial biotite and granophyre). The most obvious change is that the proportion of feldspar to orthopyroxene increases in going from LZ websterite, to MZ mela-gabbronorite, to UZ porphyritic gabbronorite (Fig. 10).

Hypidiomorphic facies

The porphyritic texture can grade over a few millimeters into a hypidiomorphic facies. Rocks that are almost entirely hypidiomorphic-textured retain relict porphyritic textures (e.g. Fig. 24a), suggesting that the hypidiomorphic textures formed through post-cumulus textural maturation. In hypidiomorphic-textured rocks, pyroxenes are less obviously euhedral than in the porphyritic facies, feldspar is less obviously divisible into phenocryst and groundmass variants, and the three pyroxene types (orthopyroxene, clinopyroxene, and pigeonite, mostly inverted) tend to form a massive interlocking texture with plagioclase (e.g. Fig. 24c). Nonetheless, sodic cores in

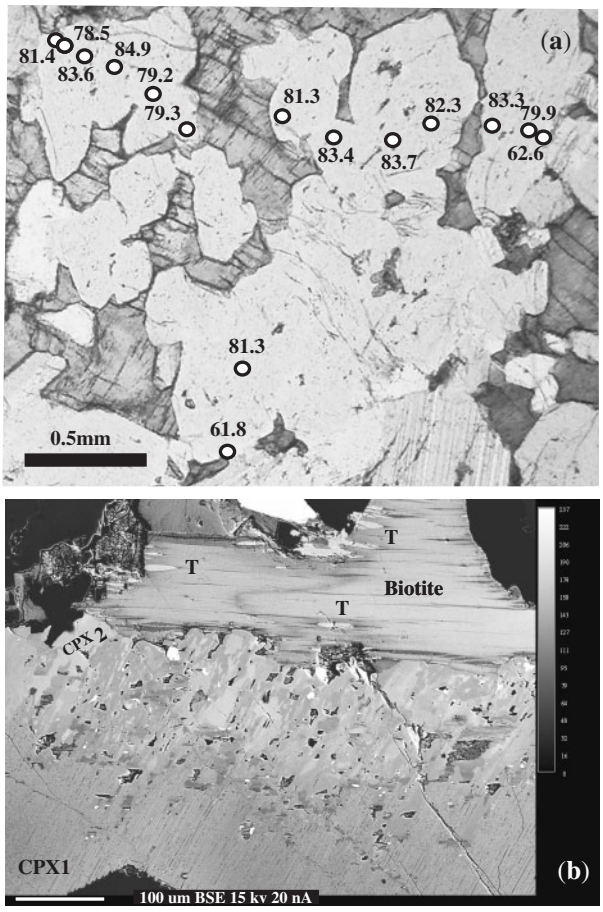

Fig. 23. Dais MZ pegmatoidal dyke 78A (see Fig. 7d). (a) Cellular-textured plagioclase grain. Numbers adjacent to spots are molar An contents. All analyzed spots are in domains with the same extinction angles and appear to constitute a single crystal. The fairly homogeneous composition, the presence of narrow sodic rims, the scalloped shape of the feldspar, and the presence of poikilitic pyroxene should be noted. Plane-polarized light. (b) Same sample. Backscattered electron image showing biotite with secondary titanite (T) growing in the cleavage, and the development of a complex secondary clinopyroxene (CPX2), intergrown with Fe–Ti oxides (bright spots), replacing an earlier generation of pyroxene (CPX1).

plagioclase still occur, as do feldspar inclusions in orthopyroxene primocrysts. Clinopyroxene, orthopyroxene and plagioclase compositional ranges overlap those of the LZ websterites and UZ porphyritic gabbronorite facies, but extend to more evolved compositions (e.g. sample 52 in Figs 15–17). Inverted pigeonite has a variety of exsolution habits (Fig. 24), and occurs as complex inter- and overgrowths of orthopyroxene and clinopyroxene (Fig. 24), or as large oikocrysts. Although pigeonite seems to replace orthopyroxene (Fig. 24), similar textures may result from co-precipitation of phases (e.g. Hall & Hughes, 1987). There can be several per cent of interstitial Fe–Ti oxides, biotite, quartz, alkali feldspar (locally as granophyric intergrowths), and minor hornblende. Incipient deuteric hydrothermal alteration is very common.

Ferrogabbroic pegmatoids

The centimeter to meter-scale ferrogabbroic pegmatoids are typically orthopyroxene-free. Clinopyroxene and pigeonite (locally inverted) are prismatic to acicular (up to 3–4 cm long), and are intergrown with euhedral plagioclase. Sodic plagioclase cores have not been observed. Pyroxene and feldspar compositions are systematically more evolved than in adjoining UZ gabbronorites (Figs. 15–17). Brown to green hornblende can form euhedral prisms, or occur as rims on pyroxene. Large interstitial patches of Fe–Ti-oxide minerals exhibit complex exsolution textures. Minor sulphide (pyrite + pyrrhotite) is present, and is generally rimmed by magnetite. Brown biotite is abundant, and may rim Fe–Ti-oxides. Chlorite rims to biotite are locally prominent. Secondary titanite may occur between biotite and clinopyroxene. Interstitial granophyre, quartz and alkali feldspar may be abundant.

A discrete 'incipient cellular textured' plagioclase base to a ferrogabbro pegmatite pod (Fig. 7c, sample 101) has feldspar laths aligned in a subhorizontal direction, and is of uncertain origin (Geist *et al.*, 2005). This sample (101) is characterized by abundant euhedral plagioclase that displays complex internal zonation (Figs 28 and 29), but that has domains much more calcic than is typical of the usual ferrogabbro pegmatites. Some feldspar grains contain inclusions of sodic feldspar (Fig. 29), whereas others seem to be veined by clinopyroxene (Fig. 28a), and appear somewhat similar to the 'cellular-textured' plagioclase from the rhythmically layered sequences (see above, Fig. 22). Clinopyroxene, orthopyroxene, pigeonite and hornblende are interstitial to oikocrystic in texture. Interstitial hornblende may be intergrown with mica. Large patches of interstitial ilmenite + magnetite envelop plagioclase.

THERMOMETRY AND OXYGEN GEOBAROMETRY

The Ca-in-orthopyroxene thermometer of Brey & Köhler (1990) was applied, for $P = 1$ kbar, to calculate maximum and average temperatures (Electronic Appendix Table A3, Fig. 30). The relatively constant values, generally between 1200 and 1280°C, should be noted. Slightly lower values were obtained for orthopyroxene-bearing veins in cellular-textured plagioclase (sample 63), and late orthopyroxene overgrowing neoblastic plagioclase (sample 70B-nb). Textural evidence indicates that orthopyroxene and high-Ca clinopyroxene (Cpx for short) are not generally in equilibrium. Where analyses are available for points in close proximity that have a good probability of having been in equilibrium, Mg = Fe exchange temperatures

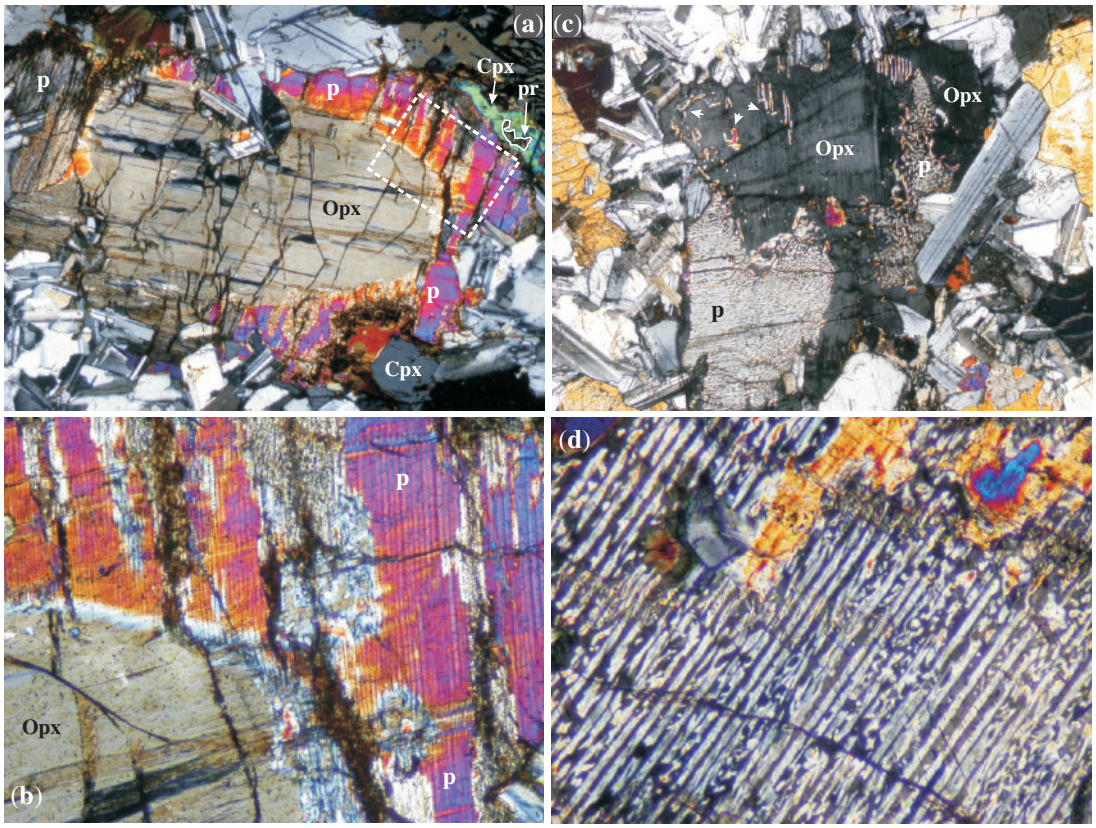

Fig. 24. (a) WBP UZ gabbronorite 52. Euhedral orthopyroxene primocryst (Opx) with partial inverted pigeonite reaction rim (p), which is in turn partly enveloped and replaced(?) by clinopyroxene (Cpx). The relict(?) inverted pigeonite bleb (pr) in the clinopyroxene rim should be noted. Field of view is 4 mm. Box indicates area of (b). (b) WBP UZ gabbronorite 52. Detail of mixed vermicular and lamellar exsolved inverted pigeonite. Field of view is 1 mm. (c) WBP UZ gabbronorite 55. Subhedral orthopyroxene (Opx) with partial rim of vermicular and pointillist-textured inverted pigeonite (p). It should be noted that the inverted pigeonite forms a partial inner ring (arrows). (d) Dais UZ gabbronorite 73. Detail of exsolved inverted pigeonite. Field of view is 1 mm. All images with crossed Nicols.

were generated (Brey & Köhler, 1990). These are uniformly low (<1150°C), with very low values (<1000°C) corresponding to the veins in cellular-textured plagioclase (sample 63), the interstitial pyroxenes in the pressure shadow of Fig. 2la and b (sample 70B-lgn-PS), and other interstitial-textured pyroxenes (samples 8l-w, 70B-lgn, 70C-lgn and 101-pg/ce). Most attempts to apply the QUILF thermometer (Andersen *et al.*, 1993) to three coexisting pyroxenes failed, with the few determinations obtained giving results similar to those of the two-pyroxene Mg = Fe exchange thermometer. The hornblende–plagioclase thermometer of Blundy & Holland (1990) yielded reasonable igneous temperatures between 1150 and 800°C for interstitial-textured amphiboles from the UZ ferropegmatoidal pods. Two-feldspar temperatures were determined (Wen & Nekvasil, 1994) using average orthoclase compositions from interstitial granophyre, or from veinlets in cellular-textured plagioclase, combined with the most sodic plagioclase analyzed in any given rock. These yield uniformly low temperatures (726–632°C), corresponding to the granitic minimum. Fe–Ti-oxide thermometry and oxygen barometry imply that ilmenite + magnetite cosaturation–exsolution began at *c.* 950°C and continued into the subsolidus (Fig. 30). Most f_{O_2} determinations (Table A3) are near the quartz–fayalite–magnetite (QFM) buffer (±2 log units), with two pegmatoids yielding more reduced solutions ($\triangle$QFM *c.* −4).

DISCUSSION

Mineral-chemical variations linked to texture in cumulus phases

Orthopyroxene

Orthopyroxene primocrysts from typical LZ, MZ and UZ gabbronorites and LZ websterites share many features: (1) most are sub-euhedral to euhedral; (2) they commonly contain plagioclase inclusions; (3) they appear to be partly replaced by clinopyroxene and locally (UZ) by pigeonite; (4) they all have similar compositional ranges (Fig. 15)

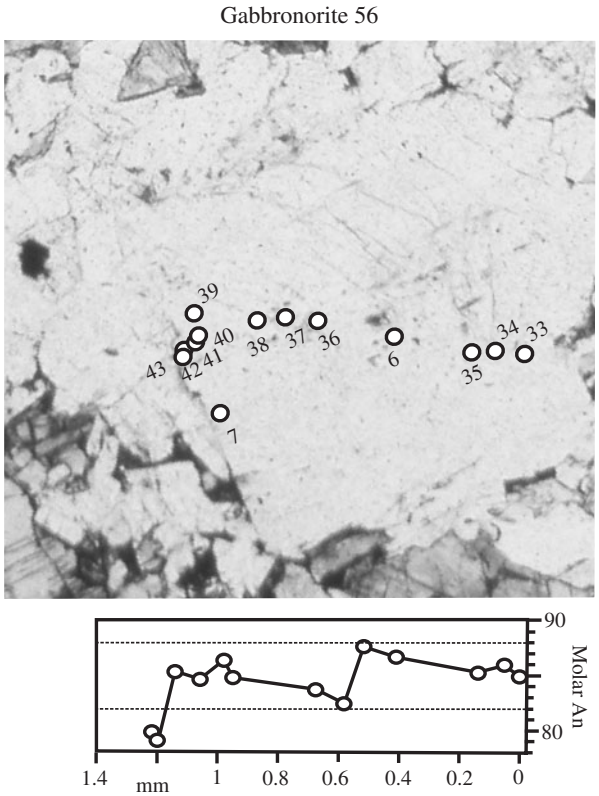

Fig. 25. Electron microprobe traverse and corresponding photomicrograph across feldspar phenocryst from WBP UZ gabbronorite 56.

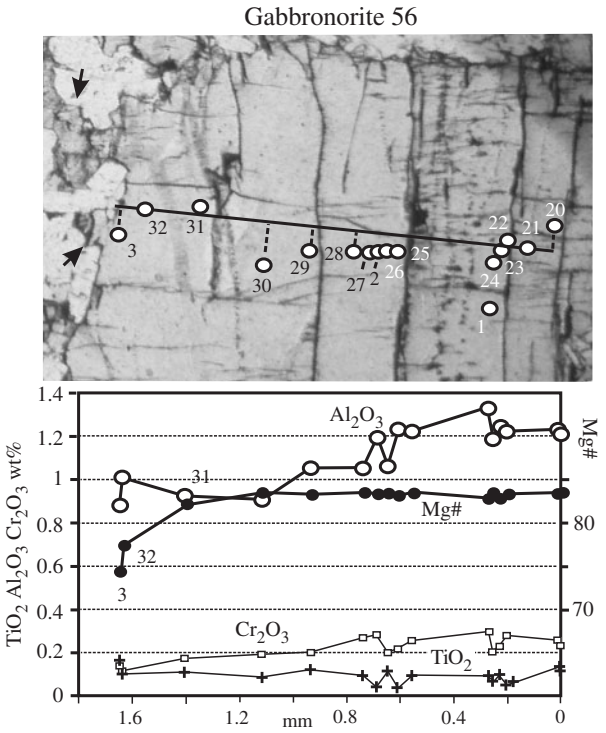

Fig. 26. Electron microprobe traverse and corresponding photomicrograph across an orthopyroxene phenocryst in WBP UZ gabbronorite 56. This is the same grain as mapped in Fig. 27. The irregular adcumulate overgrowths that occupy the spaces between groundmass plagioclase (arrows) should be noted. This crystal shows a near-constant Mg-number in the core, with a fairly systematic outward decrease in Al_2O_3 and Cr_2O_3. In contrast, TiO_2 shows significant increase only in the outermost rim and overgrowths.

that match the composition of micro-phenocrysts in the chilled margin (sample 161); (5) all yield similar Ca-in-orthopyroxene temperatures (Fig. 30). When the textures are considered together with the map-scale field evidence (Marsh, 2004), the simplest explanation for the origin of these prismatic orthopyroxene primocrysts in the Basement Sill is that they represent phenocrysts, carried in as a high-temperature (*c.* 1250°C) crystal slurry, as proposed by Gunn (1966), Marsh (1996, 2004), Marsh *et al.* (2005) and Charrier & Marsh (2004, 2005).

Zoning patterns in the orthopyroxene primocrysts can be complex (Fig. 11), with inner cores with high Cr_2O_3 and Mg-numbers that may predate saturation in feldspar, aluminous zones associated with incorporation of plagioclase inclusions (and possible resorption of plagioclase?), and broad FeO-rich rims. In contrast, TiO_2 enrichment is limited to the outermost edges, and is most marked in epitaxial overgrowths or interstitial protuberances. Because FeO diffuses more quickly than TiO_2, a simple explanation for this decoupling might be that post-cumulus re-equilibration of Fe–Mg with trapped melt (see Barnes, 1986) has penetrated more deeply into primocrysts than has re-equilibration of slowly diffusing TiO_2.

Plagioclase

The origin of the cellular-textured facies will be discussed later. We concentrate here on the common LZ websterites, MZ and UZ gabbronorites, MZ layered leucogabbronorite sequences, and LZ felsic pods and schlieren. The first-order observation for essentially all of these rocks is that plagioclase inclusions in orthopyroxene primocrysts have the same compositional range as plagioclase phenocrysts (>1 mm) and 'groundmass' laths (<1 mm, Fig. 16). This similarity between plagioclase crystals of differing paragenesis implies that these three types of plagioclase represent a single population of crystals. There are two caveats to this generalization: (1) evolved, low-temperature (Fig. 30) sodic rims are more commonly developed in phenocrysts and groundmass plagioclase that remained exposed to evolving interstitial melt, as opposed to plagioclase inclusions in orthopyroxene that were protected from such evolved melts; (2) smaller crystals may have had a shorter growth history, and so tend to record only the later stages of melt evolution (i.e. to have only normal zoning). In contrast, phenocrystic plagioclase displays complex internal zonations that reflect an equally complex

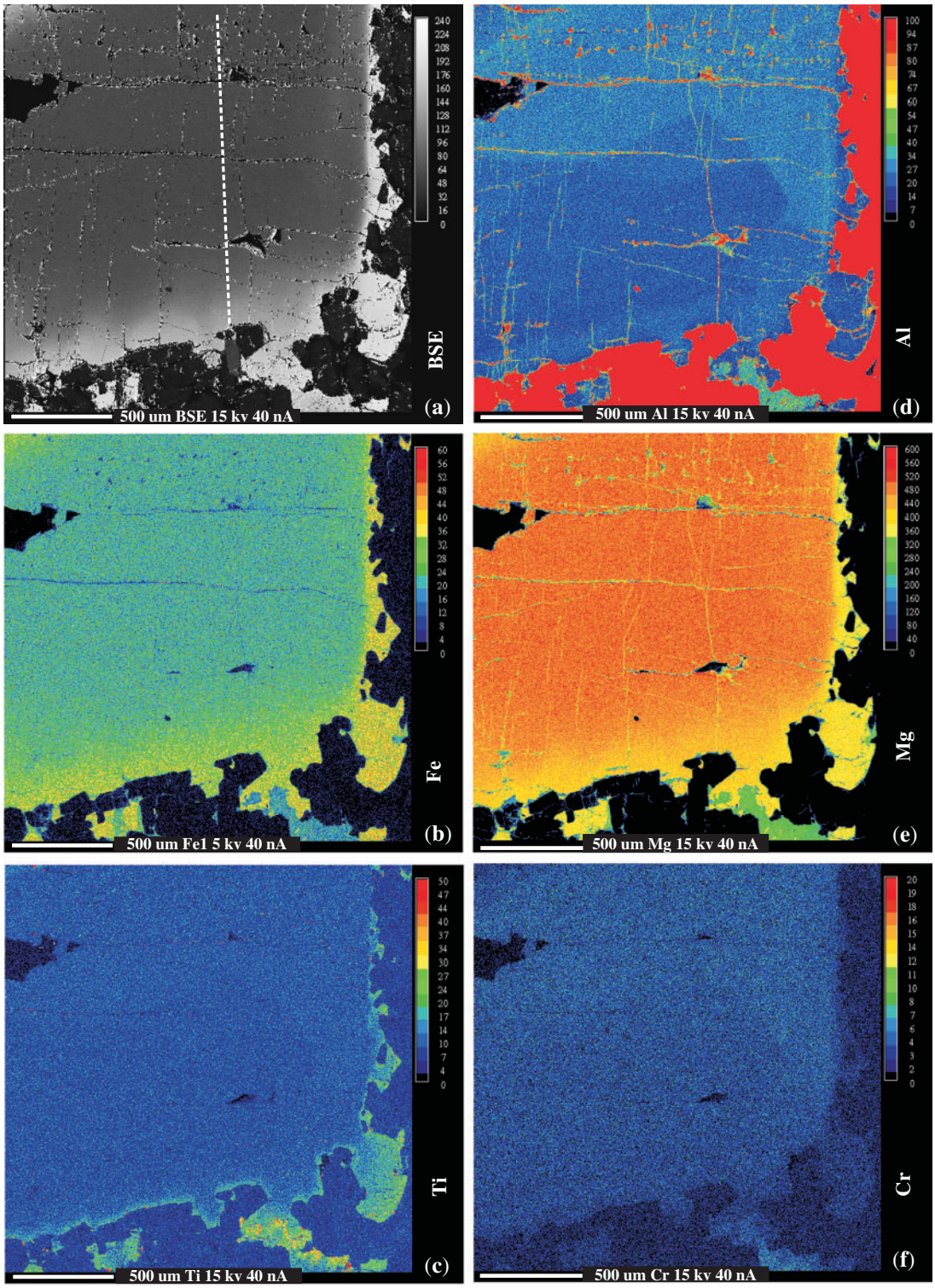

Fig. 27. Element maps for an orthopyroxene primocryst from WBP UZ gabbronorite 56. (See Fig. 12 for details of analysis.) (a) Backscattered electron image (BSE). The white dashed line is the microprobe traverse from Fig. 26. (b) Fe, (c) Ti, (d) Al, (e) Mg, and (f) Cr concentration maps. The broad zone of concentric Mg depletion and Fe enrichment (b and e) is decoupled from the very narrow zone of Ti enrichment (c), which is restricted to the rim and overgrowths. Al (d) seems to define angular domains, suggesting sector-zoning.

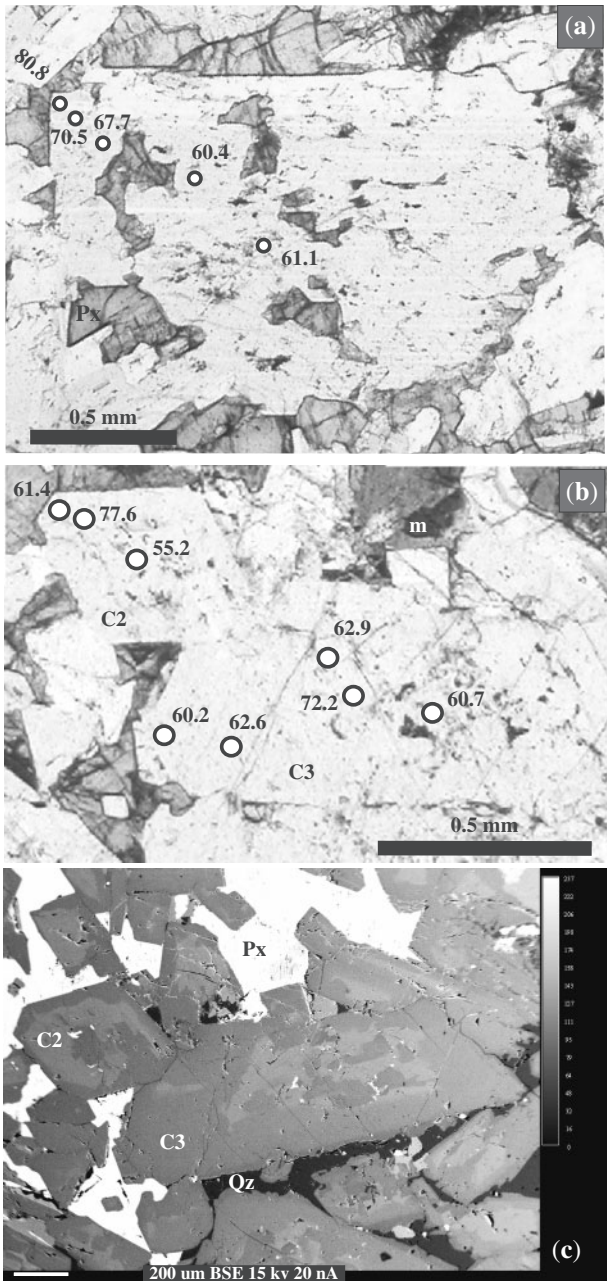

Fig. 28. Incipient cellular plagioclase grain from base of Dais UZ pegmatoid 101 (see Fig. 7c). Px, pyroxene; m, mica; Qz, quartz. (a) Photomicrograph of cellular-textured phenocryst C1 with pyroxene 'veins' inside. (b) Photomicrograph and (c) backscattered electron image showing the complex zoning patterns in phenocrysts C2 and C3. The abundant interstitial quartz (Qz) should be noted.

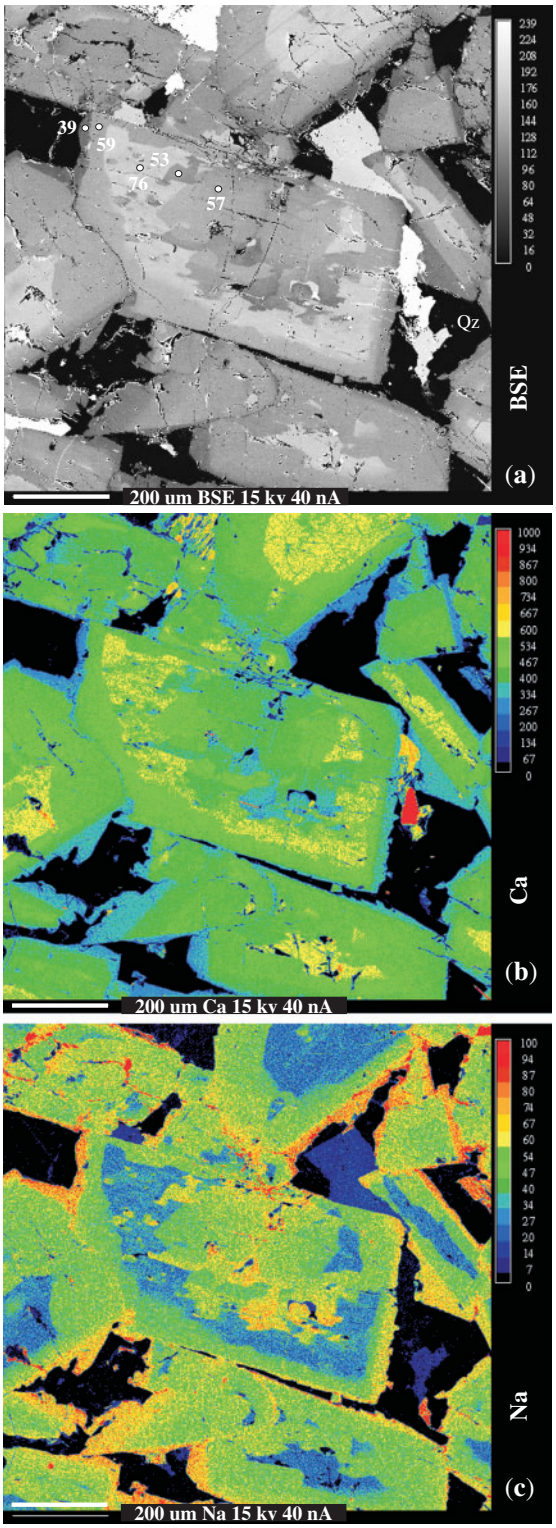

Fig. 29. Element maps from base of Dais UZ pegmatoid 101. (See Fig. 12 for details of analysis.) (a) Backscattered electron image of abundant plagioclase (prisms) with interstitial ilmenite, pyroxene, apatite and quartz (Qz). Numbers show An contents for plagioclase phenocryst C4. (b) Ca and (c) Na maps. (Note the complex zoning patterns in plagioclase.)

history (Figs 11, 13, 14, 19 and 25). For example, feldspar phenocryst C1 shown in Figs 13 and 14 has a sodic inner core, a weakly reverse-zoned outer core, a weakly normally zoned mantle, and a strongly normally zoned outer rim.

Let us first consider the origin of the strongly normally zoned outer rims, which locally reach very sodic

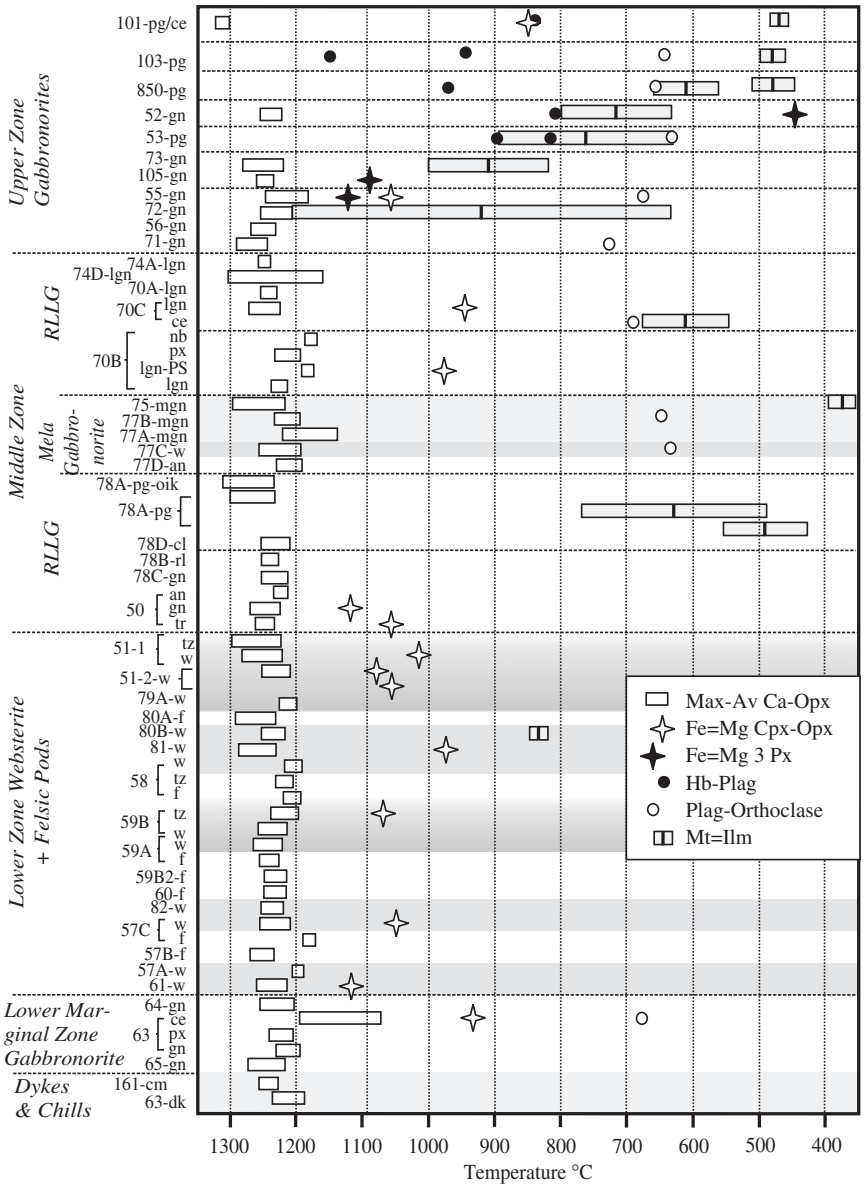

Fig. 30. Ca-in-orthopyroxene and Fe = Mg exchange temperatures calculated according to Brey & Köhler (1990), assuming 1 kbar pressure. The Fe = Mg two-pyroxene exchange temperatures were calculated only for spot analyses of grains that were in direct contact. Multi-pyroxene and oxide equilibria from QUILF (Andersen *et al.*, 1993) were calculated at 1 kbar. Most of the oxide temperatures were calculated from the Ti-exchange, magnetite–hematite, and Fe = Mg exchange reactions. Sample 73 shows results for equilibrium between three pyroxenes, hematite component in ilmenite and quartz equilibrium (QUILF). Sample 850 shows two results, one for the average magnetite and ilmenite, and another for a single datum of a high-Ti magnetite. Sample 78A also shows two results, corresponding to two types of magnetite seen in this sample, a high-Ti (high-temperature) type and a low-Ti (low-temperature) type. Results for samples 72 and 75 are based on few analyses and are not robust. The sample 75 magnetite is a narrow rim on a large ilmenite, which is consistent with the low temperature. The determination for sample 80B is based only on the Fe = Mg Mt = Ilm exchange reaction. Two-feldspar temperatures from Wen & Nekvasil (1994; SOLVCALC) use average orthoclase and the most sodic plagioclase present, either rims on laths, or in the granophyre itself. The average temperatures from the two solution models produced by the hornblende–plagioclase thermometer from Blundy & Holland (1990) are shown, for 1 atm. Sample 103 shows two results: the first is for a touching plagioclase–hornblende pair and the second is for the average amphibole composition.

compositions (Fig. 16). This extreme compositional evolution, combined with the presence of interstitial granitic minerals (quartz, alkali feldspar, biotite, ilmenite) implies that the pore melt fractionated *in situ* to reach 'granitic' compositions at *c.* 700–650°C (Fig. 30). Typically, these outer sodic feldspar zones are extremely narrow, reflecting the known resistance of plagioclase to diffusional re-equilibration. Some of the smaller groundmass laths,

on the other hand, have wider sodic outer zones (Fig. 14), and a larger proportion of their volume (20–30%) must have crystallized directly from these evolved pore melts after the crystal framework locked up and started evolving as a closed system.

In contrast, most of the volume of plagioclase phenocrysts, groundmass laths and inclusions in orthopyroxene, have near-constant compositions (An82–86: Fig. 16), with only weak normal or reverse zoning (e.g. Fig. 13 grains C2 and C3, and Fig. 19). The near-constant compositions imply that these crystals grew under nearly isothermal conditions from a large body of melt that may have evolved slightly as a result of either progressive crystallization (weak normal zoning) or replenishment (weak reverse zoning). Extraction of this much plagioclase by progressive fractional crystallization from a body such as the Basement Sill should have resulted in more extensive plagioclase compositional variation than is observed. One possible resolution of this conundrum is that most of the plagioclase grew in a large holding chamber at depth, was mechanically concentrated, and then emplaced as a slurry (together with orthopyroxene) into the Basement Sill.

As pointed out above, the only obvious textural difference between the small 'groundmass' plagioclase laths and small plagioclase laths that are embedded in orthopyroxene is that the latter rarely show facets. There are two possible explanations for this observation. (1) Included plagioclase laths were originally euhedral, with rounding representing a subsolidus adjustment of grain boundaries (Hunter, 1987; Holness *et al.*, 2007). (2) Rounding is due to magmatic resorption immediately prior to incorporation into the growing orthopyroxene (see Eales *et al.*, 1991; Tegner *et al.*, 1996). Although we cannot exclude the first hypothesis, the association of feldspar inclusions with Al_2O_3-enriched growth zones in the orthopyroxene primocrysts (FIZ in Fig. 11) seems more consistent with the second hypothesis. This implies that a feldspar-enriched melt mixed with a pyroxene-enriched feldspar-undersaturated melt at some stage. The ubiquity of feldspar inclusions in Basement Sill orthopyroxene primocrysts implies that this mixing event probably predates injection of the crystal-charged slurry into the Basement Sill.

A significant proportion of samples contain plagioclase with anhedral sodic plagioclase cores that are associated with Fe-rich clinopyroxene, quartz, ilmenite, orthoclase and mica (Fig. 13 grain C1, Figs 14 and 16). There are two possible explanations for the presence of such sodic cores and the associated minerals. As suggested by Pietranik *et al.* (2006), they may represent a dissolution–precipitation reaction-product generated as evolved pore melt preferentially reacted with a calcic inner core that was in gross disequilibrium with the pore melt. We do not favour this hypothesis because: (1) the sodic outer rims form clean overgrowths (Fig. 14) with not a hint of excavation or infiltration; and not a single example of a channel linking the groundmass to one of these sodic inner cores has been observed to date; (2) the plagioclase mantles (An *c.* 87–85) are equally out of equilibrium, but show little sign of reaction or replacement. We prefer to interpret the sodic inner cores as near-cognate 'xenocrysts' and 'xenoliths' derived from partial digestion of a gabbroic cumulate at depth.

The absence of cryptic mineral variations suggests mechanical redistribution of phases

Perhaps the most striking feature of the mineral-chemical profiles (Figs 15–17) is the extremely modest range of cryptic variation throughout the LZ, MZ and UZ of the Basement Sill. Maximum and average orthopyroxene Mg-number and Cr_2O_3 content are uniformly high in all facies, with compositions similar to those observed in micro-phenocrysts from the chilled margin (sample 161, Figs 8 and 15). Modest variations of Mg-number and Cr_2O_3 content are consistent with *in situ* fractionation of abundant trapped melt (20–30%: Bédard *et al.*, 2005). Similarly, plagioclase feldspar shows little or no systematic cryptic variation in An-content (Fig. 16), with all facies containing feldspars with An contents *c.* 85, a composition similar to that of euhedral micro-phenocrysts from the chilled margins (samples 161 and 63-3, Fig. 16). There is a hint of an increase in An content from the base to the top of the LZ (Fig. 16a), but the increase is very subtle and may reflect the small number of samples analyzed from the base of the LZ.

Departures from this uniform mineral-chemical signature are seen only in: (1) ferrogabbroic pegmatoids (samples 53, 78a, 101, 103, 850), which appear to record movement and emplacement of low-temperature residual melt and fluid; (2) the LMZ gabbronorites (samples 64 and 65), which could have crystallized from a distinct melt, or where the pyroxenes might have experienced more extensive post-cumulus re-equilibration with trapped melt as a result of finer grain sizes and more extensive trapped melt fractions; (3) the unusual cellular-textured domains (samples 70A, 70B and 63-2) and associated impregnation facies that we interpret as being due to movement of late, low-temperature, evolved melt fractions (e.g. sample 70C); (4) post-cumulus orthopyroxene grains in pyroxene-poor facies (samples 50-tr, 50-an, 51-1-f and 57C-f) which probably reflect a combination of *in situ* fractional crystallization and late enrichment as a result of reaction of Fe-rich trapped melt with scarce pyroxenes; (5) anhedral cores in phenocrysts that probably represent xenocrysts, reflecting an earlier differentiation event at depth.

Clinopyroxene (and pigeonite) are typically late-crystallizing phases that show little systematic evolution with

stratigraphic height (Fig. 17) from the base of the LZ to the middle of the UZ. The LMZ gabbronorites have more evolved clinopyroxenes, and may have crystallized from a slightly more evolved melt, an inference that is in accord with the more evolved compositions of feldspars and orthopyroxenes from these rocks. Some UZ gabbronorites also have more evolved clinopyroxene compositions. This might reflect the systematic upward migration of evolved pore melt caused by compaction. The abundance of Fe-rich pyroxene, quartz, ilmenite and orthoclase in the cellular-textured, pegmatoidal and metasomatic facies implies that the pore melts were indeed enriched in FeO, TiO_2, alkalis, SiO_2 and H_2O. The upward concentration of the percolating pore melt would mostly have affected the late-crystallizing clinopyroxene and groundmass plagioclase, without significantly resetting feldspar cores or orthopyroxene primocrysts, the compositions of which would largely have been inherited from the original infilling event.

Thus, to a first approximation, the dominant facies from the Basement Sill all contain the same population of orthopyroxene and plagioclase, albeit in different proportions. This is clearly inconsistent with models involving sequential accumulation of crystals and bottom-to-top fractional crystallization. In other words, the uniformity of mineral-chemical compositions and temperatures implies that the gross zonation into websterite or gabbronorite (LZ or UZ) exhibited by the Basement Sill does not reflect sequential extraction of orthopyroxene (websterite cumulate) followed by co-saturation in plagioclase (norite), and then Ca-rich clinopyroxene (gabbronorite). When one also considers the clear textural similarity of UZ gabbronorite and LZ websterite (e.g. Fig. 10), and the evidence for early co-saturation in plagioclase + orthopyroxene (Figs 10 and 11), then the simplest explanation for the evidence is that most of the orthopyroxene and plagioclase were injected together as a slurry, and then mechanically unmixed in response to buoyancy forces. Given the scale of the Basement Sill (*c.* 400 m), this implies that a mushy zone of this thickness once existed, and that mechanical unmixing of phases can occur on this scale. Pyroxenite–gabbroic cyclic layering in the Bushveld Complex has a similar scale. In a series of papers, Eales *et al.* (1991) and Cawthorn (2002) developed models involving retention of plagioclase in the fractionating melt as a result of its neutral or positive buoyancy, with preferential deposition of denser pyroxene at the base. However, because of the extensive post-cumulate re-equilibration of textures in the Bushveld Complex, the detailed manner in which the retention–deposition processes functioned remains obscure, and so this model has not gained universal acceptance. The evidence from the Ferrar Basement Sill presented here provides support for the type of model advocated by Eales *et al.* (1991) and Cawthorn (2002), and adds important observations about the way in which melt and mineral phases were redistributed to generate the first-order lithological differentiation that is observed.

Field evidence implies that the felsic pods and schlieren that occur throughout the Basement Sill LZ are segregation structures of some type. For the six occurrences of coexisting felsic pods and schlieren and host websterite that we analyzed (samples 80A-80B, 58, 59B, 59A, 57C and 57B-57A), mineral-chemical data show that plagioclase from the felsic pods and schlieren is indistinguishable from plagioclase in the adjoining websterite (Fig. 16). Orthopyroxene primocrysts and clinopyroxene in the felsic pods are very slightly more evolved than those in the adjoining websterite (Figs 15 and 17), but the differences are small, and can probably be accounted for by the trapped melt effect acting on rocks with different pyroxene/plagioclase ratios (Barnes, 1986; Cawthorn *et al.*, 1992). This mineral-chemical similarity implies that the felsic pods and schlieren did not crystallize from pools of fractionated melt segregated after extensive crystallization of websterite, because they would then be characterized by systematically more evolved mineral compositions, and would presumably show different textural characteristics. The close similarity of textures, mineral compositions and calculated temperatures, and the field evidence for 'rooting' of felsic schlieren in websterite suggest to us that the felsic pods and schlieren represent partial expulsion and reconcentration into channels of the feldspar-charged melt separating orthopyroxene primocrysts in the websterite. The close resemblance of mineral chemistry and textures of the larger felsic pods to those of UZ gabbronorites further suggests that the feldspar-charged melt expelled from the LZ websterite travelled up to feed the UZ.

The layered leuco-gabbronorite sequences of the MZ are laterally discontinuous, and are embedded in mela-gabbronorite that appears to be transitional between LZ websterite and UZ gabbronorite. As a whole, MZ leuco-gabbronorite has a high plagioclase/orthopyroxene ratio and textures and mineral chemistry (Figs 15 and 16) that are very similar to those seen in the felsic pods and schlieren of the LZ. A simple explanation (albeit speculative) for these features, and for why layered leuco-gabbronorite sequences occur in this part of the stratigraphy (Figs 3 and 4), is that the layered leuco-gabbronorites formed from ascending, channelized, feldspar-charged slurries that stalled at these levels to form intra-cumulate sills (Fig. 31). In such a model, much of the 1–5 m scale layering in these sequences would represent internal intrusive contacts. In this interpretation the layered leuco-gabbronorite sequences are not true rhythmic depositional beds, but represent composite sills complexes (see Bédard *et al.*, 1988; Bédard, 1991). Flow-differentiation within these sills would also account for the presence of finer-grained

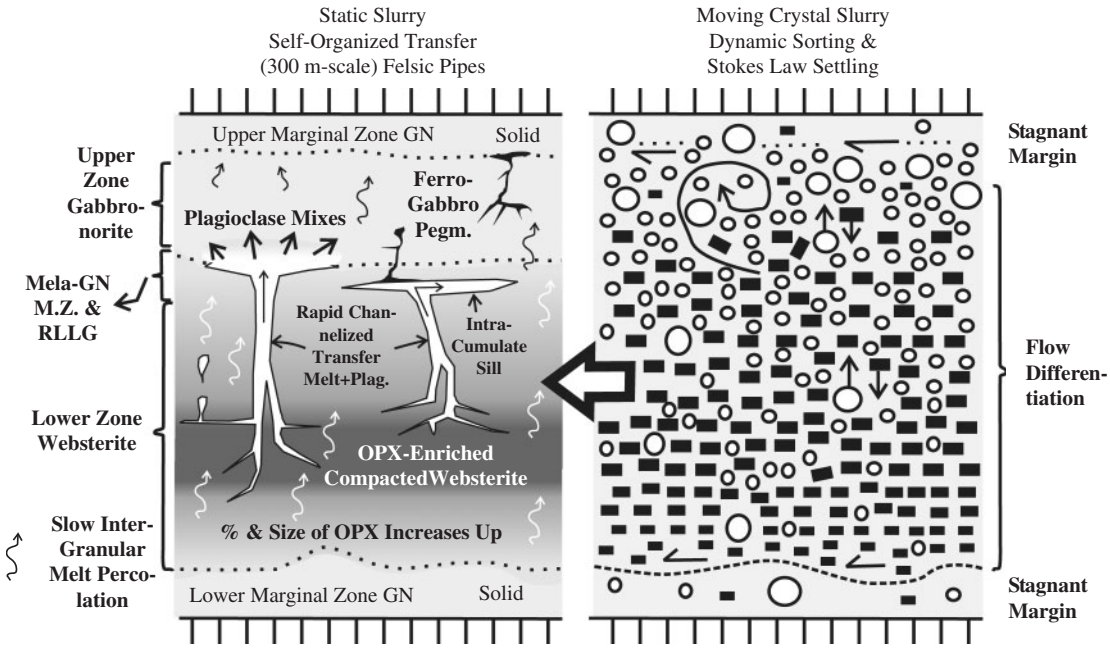

Fig. 31. Schematic illustration of the model advocated here. The panel on the right shows the slurry influx stage, where flow differentiation concentrates crystals in the intrusion core, while buoyancy forces tend to concentrate feldspar ({cir}) towards the top, and orthopyroxene (black rectangles) towards the base. The panel on the left shows the processes active after the slurry stops moving. Transfer of feldspar-charged residual melts would have occurred mainly through a network of channels or possibly as diapir trains (white); this would have been superimposed on a diffuse upward percolation of evolved residual melt (squiggly arrows). Local concentrations of evolved Fe–Ti-rich melt generate pegmatoids (black).

orthopyroxene primocrysts at both upper and lower contacts of layers, with coarser orthopyroxene primocrysts characterizing the center of layers.

A possible scenario for mechanical segregation of phases in the Basement Sill

The textural and mineral-chemical evidence suggests that orthopyroxene and plagioclase were both present in the crystal-rich slurry that filled the Basement Sill. However, we have few constraints on the initial plagioclase/orthopyroxene ratio, or on the internal organization of the incoming slurry. It may have been well mixed, or there may already have been a cloud of buoyant plagioclase riding atop an orthopyroxene-rich bedload (Fig. 31) as a result of dynamic sorting effects (see Irvine, 1980). Deposition of multi-mineral slurries with different grain-size distributions along the flanks or ahead of the expanding slurry is likely to be extremely complex, and could account for some of the faint layering seen in this body.

Marsh (2004), Petford *et al.* (2005) and Sumita & Manga (2005) suggested that the thinner feldspathic schlieren in the LZ websterite might initially have formed as dilation zones in a crystal-charged slurry, with the fine-grained plagioclase (+ melt) migrating into low-pressure zones. Granular materials do not shear homogeneously like fluids, but most often form rigid regions separated by narrow shear or slip bands (e.g. Nedderman, 1992; German, 1989). At near maximum packing, shear causes local dilation in narrow zones into which small grains selectively migrate to form distinct bands of segregated grains. Shear most often sets in where porosity is slightly higher, which may be due to local packing characteristics, particle shape or concentration. When the regions of larger grains are relatively locked, the bands will remain thin, but if the large grains are packed loosely enough also to participate in the shear, the shear zone could grow significantly wider, perhaps almost without limit (Fenistein & van Hecke, 2003).

On the other hand, the larger felsic pipes with paleovertical elongations clearly post-date this lateral flow–infilling event (Figs 6 and 18a). Thus, it seems reasonable to assume that, at some juncture, the partly differentiated crystal-rich slurry slowed and stopped, and that subsequent mass-movements were dominantly vertical. If the initial porosity was high, it seems probable that single orthopyroxene and plagioclase phenocrysts could have have moved independently (Stokes' Law settling or variants thereof: Martin & Nokes, 1989; Koyaguchi *et al.*, 1993). However, once the crystallinity exceeded a critical threshold (perhaps *c.* 25–35%), then single crystals could no longer have moved independently and alternative scenarios need to be considered (e.g. Simura & Ozawa, 2006).

Field, textural, and mineral-chemical evidence from the Basement Sill leads us to suggest that much of the feldspathic component that was injected into it was transferred towards the top of the immobilized sill though channelized flow (Fig. 3l), or as intermittent diapirs (see Hoshide *et al.*, 2006*a*, 2006*b*). In this model, as the orthopyroxene-rich framework of the LZ cumulates compacted under its own weight, the interstitial melt (and the fine-grained plagioclase grains suspended in it) would have been expelled and concentrated into channels, layers or pools. The siliceous, hydrous melt composition means that this expelled melt would have been of low density, and so would have been prone to rise, entraining neutrally or positively buoyant plagioclase within it. Moving interstitial melt naturally tends to form channels (e.g. Bédard *et al.*, 1992; Whitehead & Kelemen, 1994; Aharonov *et al.*, 1995). The larger channels (meter-sized, Fig. 6) would end up dominating the system and could have drained the entire pyroxenite mush through a complex network of smaller (millimeter- to centimeter-sized) ramifying tributaries (Fig. 5). The vertical extent of channels in the Basement Sill at the time of segregation is unknown. It is entirely possible that the ascending feldspar-rich slurry might have moved as elongated diapirs, pinching out at the base as they propagated upwards (see Rubin, 1998). A very similar model was proposed recently for the 120 m thick Nosappumisaki intrusion (Simura & Ozawa, 2006), and for the 220 m thick Murotomisaki gabbroic complex (Hoshide *et al.*, 2006*a*, 2006*b*).

As the porosity decreased in the lee of the escaping feldspar-rich magma, the orthopyroxene primocrysts would begin to close up and reduce the permeability (Fig. 18b) to the point where it would no longer have been possible to efficiently expel the interstitial feldspar-charged melt, much of which would have remained trapped within the orthopyroxene primocryst framework (Figs 10 and 18b). Trapped interstitial magma would then have crystallized and fractionated *in situ* to generate (1) sodic rims on feldspar and Fe-rich rims on orthopyroxene primocrysts (e.g. Figs 12 and 14) and (2) interstitial clinopyroxene + ilmenite + quartz + orthoclase + mica (granite). Preliminary estimates derived from inverse geochemical modeling suggest that the residual porosity of most Lower Zone websterite cumulates was 20–30% (Bédard *et al.*, 2005). Compaction beyond this point is thought to require the application of shear stresses (e.g. Dick *et al.*, 1991; Bédard *et al.*, 2003). Although localized internal deformation structures occur in the Basement sill (Fig. 5c), they are rare, and probably did not greatly increase the sill's overall fractionation efficiency.

The origin of websterite intrusion 77C (Fig. 7b) is possibly linked to channelized ascent of the feldspar-rich melt. Websterite 77C was emplaced into an MZ mela-gabbronorite septum between two layered leuco-gabbronorite sequences. A metasomatic origin seems inconsistent with the orthopyroxene compositions (Fig. 15) and primocryst zoning patterns seen in this rock, which are similar to those of LZ websterites. If it was emplaced as an orthopyroxene-rich slurry, then its high density should have precluded a gravity-driven ascent mechanism. A speculative explanation is that this websteritic intrusion represents siphoning of orthopyroxene primocrysts into the tail end of a draining gabbronoritic pipe. Because of the upward suction force that would have been exerted by the ascending feldspathic slurry in a feldspathic pipe, a low-pressure zone may have developed in its lee, and when easily accessible feldspar-rich melt was exhausted from the source volume, poorly consolidated orthopyroxene primocrysts could have been drawn into the pipe to fill the void left by the rising plagioclase-rich melt.

Because the Basement Sill is fairly thin, it is plausible to suggest that rapid cooling is responsible for fossilization of the melt drainage channels decribed above. This might not be the case in larger layered intrusions, where slower cooling rates might not allow preservation of transient melt escape structures (see Helz *et al.*, 1989). We suggest that a similar mechanical segregation history to what we have documented for the Ferrar Basement Sill may also characterize the Bushveld Complex Critical Zone, and speculate that as the felsic material drained out of the Bushveld pyroxenite, the pyroxene-rich mush flowed inward and pinched out the ascending felsic pipes at their base, leaving little trace of their previous existence.

Timescale for segregation–deposition

The bottom-line constraint for such a channelized mechanical redistribution model (Fig. 3l) to be plausible is that the time needed to transfer an appropriate volume of plagioclase-charged mush from the LZ to the UZ must be less than the solidification time of the sill. The purpose of the calculations that follow is to verify if this is possible. In the model certain simplifying assumptions have been made. We assumed that the effective thickness of the Basement Sill at the time the slurry arrived was about 300 m (excluding the UMZ and LMZ), and that all of the orthopyroxene in the LZ represents entrained primocrysts that settled out in some way. We do not know what the proportion of orthopyroxene to feldspar was in the incoming slurry, but typical LZ websterites contain *c.* 50–60% orthopyroxene, and inverse models (Bédard *et al.*, 2005) suggest that the LZ websterites contain *c.* 20–30% trapped melt, which implies that LZ websterites now contain *c.* 10–25% 'cumulus' plagioclase. For the modeling, we assumed that the felsic pipes formed when the compacting orthopyroxene + feldspar slurry had a porosity of about 45%, which corresponds to a crystal fraction that precludes Stokes' Law settling of crystals. The time taken to transport interstitial melt (and suspended plagioclase laths) upwards from the LZ cumulates through melt-rich

pipes is estimated based on the number density of pipes and their radii measured in the field (Fig. 6c), reasonable estimates of melt viscosity, and the relative volumes of interstitial melt and orthopyroxene primocrysts in the LZ websterite. The volume flux of magma through a single pipe by laminar flow is

$$Q = \pi \Delta \rho g a^4 / 8\mu \quad (1)$$

where $\Delta\rho = 10^2\,\mathrm{kg/m^3}$ is a conservative estimate of the density contrast between magma in the pipes and the orthopyroxene-rich magma of the LZ, a is the pipe radius, g is the gravitational constant, and $\mu = 10^{1.5}\,\mathrm{Pa\ s}$ is the dynamic viscosity of the melt-rich pipe, assuming a suspension of 20% entrained neutrally buoyant plagioclase crystals by volume. The suspension viscosity is determined from a relation similar to Roscoe's equation and is

$$\mu = \mu o (1 - \phi)^{-2.5} \quad (2)$$

where μ_0 is the dynamic viscosity of the melt and ϕ is the crystal volume fraction relative to that at maximum packing (Marsh, 1981). The mean volume flux of magma per pipe is determined using the average of the measured pipe radii to the fourth power, $\mathrm{av.}(a^4) = 1{\cdot}33\ \mathrm{m^4}$, and not the mean pipe radius. The number density of pipes is $\mathrm{no.}/l^2 = 2 \times 10^{-3}\,\mathrm{m^{-2}}$. The volume of interstitial melt in the cumulate pile normalized by area is

$$V/l^2 = \Delta \phi L \quad (3)$$

where $\Delta\phi = 0{\cdot}45$ is the volume fraction of interstitial melt and $L = 300\,\mathrm{m}$ is the sill height. The total time for the melt to be transported is

$$t_m = (V/l^2)/(\mathrm{av.}Q \times \mathrm{no.}/l^2) \quad (4)$$

which is the area-normalized melt volume divided by the product of the mean volume flux of magma per pipe and the pipe number density. This calculation yields an extremely short timescale of $\sim 7 \times 10^4\,\mathrm{s}$, or about 8 days. This simple model assumes that the pipes are formed initially, there is no delay for interstitial melt to be transported into the pipes, and that mush compaction is not rate-limiting. If the ascending suspension contained 40% plagioclase crystals by volume instead of 20%, then the suspension viscosity, and therefore total time for melt to be transported, would be an order of magnitude larger (80 days).

This is broadly comparable with the time taken to deposit a suspended load by simple sedimentation processes. The process of sedimentation of concentrated suspensions is analytically complicated (e.g. Kynch, 1952; Barnea & Mizrahi, 1973; Davis & Acrivos, 1985; Al-Naafa & Selim, 1992), but the associated time scales are all related to multiples of Stokes' Law (e.g. Greenspan & Ungarish, 1982; Marsh, 1988). The characteristic settling time (t_2) is related to a multiple of that given by Stokes' Law for settling (V_o) through a layer distance H of a single (large) particle in melt of this composition and temperature. That is,

$$T_2 = 7H/Vo = 36.5H\mu/\Delta\rho g a^2 \quad (5)$$

where μ is viscosity ($\sim$100 p), $\Delta\rho$ is the density contrast between orthopyroxene and melt ($\sim 0{\cdot}5\,\mathrm{g/cm^3}$), g is gravity, and a is crystal radius ($\sim$5 mm). For H of 10–100 m, t_2 ~10–100 hrs, which even for 10–100 times these values represents a relatively short time.

A necessary condition for the transport of interstitial melt through pipes is that the sill does not solidify before transport can occur. For simplicity, if we assume the sill was an instantaneously injected sheet of magma that cooled conductively, then following Zieg & Marsh (2002), we can approximate the problem as one-dimensional heat diffusion in two adjacent infinite half-spaces of country rock ($-4 < \chi < 0$) and melt ($0 < \chi < 4$).

Under these conditions, the time for the temperature to pass from the liquidus to the solidus at a particular position, $\chi > 0$ is $t_c \sim \chi^2/4b^2\alpha$, where $\alpha = 10^{-6}\,\mathrm{m^2/s}$ is the thermal diffusivity and $b = 0{\cdot}6$ is a constant to account for latent heat release and the initial temperature of the country rock and melt. The time for the sill to be completely solidified, $\chi = L/2$, is then ~500 years, or over three orders of magnitude larger than the maximum time estimated to transport all of the interstitial melt in pipes (8–80 days). Based on this analysis, we conclude that it is physically possible to deposit the suspended load, and transport enough interstitial melt + plagioclase from the compacting LZ through melt-rich pipes to account for growth of UZ gabbronorites within a very small fraction of the time needed for the sill to solidify.

Expulsion of residual Fe-rich melt from gabbronorites and the origin of cellular-textured plagioclase

The textural evidence (Figs 20–22), such as neoblastic deformation zones, brittle fracture of plagioclase, overprinting metasomatic pyroxenite, and vein-like morphology of pyroxene–quartz–ilmenite–orthoclase segregations, as well as the evolved mineral chemistry (Figs 15–17) suggest that low-temperature (Fig. 30) residual melt enriched in SiO_2–FeO–TiO_2–Na_2O–K_2O–H_2O was expelled from MZ and UZ gabbronorites. The clinopyroxene-rich nature of the segregations (Figs 20–23), when considered together with the clinopyroxene-depleted nature of the MZ layered leuco-gabbronorite sequences, and the local preservation of clinopyroxene-enriched pressure shadows in MZ leucogabbronorite (Fig. 21a and b) suggest that melt expulsion typically occurred before clinopyroxene cosaturated. Field evidence (Fig. 7a and d) suggests that the evolved residual melt moved along layer contacts to concentrate into

bulbous or dyke-like bodies of Fe-gabbroic pegmatoid in the MZ and UZ.

The origin of the cellular-textured plagioclase remains problematic. Several features must be considered: (1) the cellular-textured plagioclase is only slightly more sodic than that in typical gabbronorites; (2) it envelops gabbronoritic patches with textures and mineral-chemical signatures indistinguishable from those of 'normal' gabbronorites; (3) its formation predates infiltration of the residual, low-temperature Si–Fe–K–Na-rich melt expelled from the compacting leuco-gabbronorites; (4) some cellular-textured plagioclase appears to have been eroded and entrained into later leuco-gabbronorite flow units, suggesting a repetitive process. There are also some similarities between the 'type' cellular-textured plagioclase and some of the facies associated with the Fe-rich pegmatoids (Figs 28 and 29) and the intrusive contacts in the LMZ (Fig. 9). We speculate that cellular-textured plagioclase is a proto-pegmatitic facies developed by the recrystallization of pre-existing gabbronorite under the action of a volatile-rich impregnating melt, now manifested as pyroxene-rich vein assemblages impregnating the leuco-gabbronorite (Fig. 21c and d) and intruding the cellular-textured plagioclase (Fig. 22). In the case of the MZ and UZ, these evolved melts would ultimately originate through *in situ* fractional crystallization of melt trapped between cumulus orthopyroxene and plagioclase.

The origin of the cellular-textured plagioclase in the LMZ illustrated in Fig. 9 can be interpreted in a similar manner. The neoblastic anorthosite could be linked with emplacement of the intrusion, or with slip along this internal contact during sill inflation. The cellular-textured plagioclase could record ponding of expelled evolved pore melt from the host gabbronorite against a permeability barrier represented by the fine-grained contact. It is also possible that reheating by the intrusion could have contributed to the generation of minor amounts of evolved, volatile-rich melt in the host gabbronorite. These remain speculations, however, and the origin of this distinctive texture is not yet fully explained.

CONCLUSIONS

The Basement Sill of the Jurassic Ferrar dolerites of Antarctica can be divided into a Lower Marginal Zone (LMZ) chill + gabbronorite, a thick Lower Zone (LZ) feldspathic websterite, a transitional Middle Zone (MZ) characterized by mela-gabbronorite and strongly layered leuco-gabbronorites, and an Upper Zone (UZ) composed of gabbronorite and ferrogabbroic pegmatites that grades up into an Upper Marginal Zone (UMZ) gabbronorite and chill. Textures and mineral compositions of the LZ websterite, MZ mela-gabbronorite, and UZ gabbronorite are nearly identical, the main distinction being the greater relative proportion of plagioclase, and the greater proportion of pigeonite in some UZ gabbronorites. Most orthopyroxene grains are sub-euhedral normally zoned primocrysts, commonly with plagioclase inclusions. Plagioclase is commonly sub-euhedral and normally zoned, but may contain more evolved xenocrystic cores. Clinopyroxene and pigeonite are post-cumulus phases in all except the Fe-rich pegmatoids. Orthopyroxene (Mg-number = 86–80) and feldspar (An87–82) compositions in most of the sill are similar to the compositions of micro-phenocrysts in the chilled margins, and we infer that the sill was filled by a crystal-charged slurry of plagioclase + orthopyroxene that subsequently unmixed in response to buoyancy forces. Geothermometry suggests that this influx was at *c.* 1250°C. The LZ websterites contain numerous feldspar-enriched schlieren, veins and pipes that we interpret to be fossil segregation channels. These channels are filled with anorthosite to gabbronorite with textures very similar to (1) the groundmass separating the accumulated LZ orthopyroxene primocrysts and (2) UZ gabbronorites. The mineral chemistry of these pipes is nearly indistinguishable from that of the host LZ websterite, and we infer that plagioclase-enriched pore melt expelled from the compacting orthopyroxene cumulates pooled and ascended through conduits to feed growth of the UZ. Detailed maps show that pipes are separated by about 15 m on average, and calculations suggest that this number density of conduits could have drained the websterite zone of its interstitial melt + plagioclase in about 8 days. Well-bedded leuco-gabbronorite sequences straddle the LZ–UZ transition and constitute an MZ in the Dais Intrusion. We suggest that the MZ leuco-gabbronorite may represent ponding of the ascending plagioclase-rich slurries at this interface. Fe–Ti-rich pyroxenitic veins and pods (some pegmatitic) and cellular-textured coarse-grained plagioclase occur at the contacts between some MZ layers, and ferro-pegmatites are also well developed throughout the UZ. We interpret these Fe-rich pegmatoidal rocks as evolved residual melts expelled from the compacting gabbronorite cumulates. Thus, the Basement Sill records density-driven mechanical crystal–melt unmixing on a 300–400 m scale. The pyroxenite–gabbro duality resembles that of the Bushveld Critical Zone, and we suggest that similar ephemeral magmatic processes may also have operated there (and elsewhere).

ACKNOWLEDGEMENTS

This work is partly an outgrowth of the Magmatic Field Laboratory Workshop held in the McMurdo Dry Valleys during January 2005. A report on this venture has been given by Bédard (2005). We wish to thank the National Science Foundation and the PHI aircrews and ground support personnel at McMurdo Station, Antarctica for transporting, training and maintaining our field party during the expedition. We particularly wish to thank Erika

Eschholz for keeping a herd of refractory cats out of trouble. Constructive comments from Stephen Barnes, Marian Holness, Troels Nielsen and Christian Tegner are gratefully acknowledged. The analytical data were collected with the help of Marc Choquette (U.Laval). We also acknowledge the many valuable discussions with the other members of the expedition. Fieldwork and travel were funded by NSF Grants OPP-02 29306 and OPP 0440718 to Johns Hopkins University (B.D.M.); and the analytical work by Geological Survey of Canada Ventures Project 200-303510. This is ESS Geological Survey of Canada Contribution 20070097.

SUPPLEMENTARY DATA

Supplementary data for this paper are available at *Journal of Petrology* online.

REFERENCES

Aharonov, E., Whitehead, J. A., Kelemen, P. B. & Spiegelman, M. (1995). Channeling instability of upwelling melt in the mantle. *Journal of Geophysical Research* **100**, 20433–20450.

Al-Naafa, M. A. & Selim, M. S. (1992). Sedimentation of monodisperse and biodisperse hard-sphere colloidal suspensions. *AIChE Journal* **38**, 1618–1630.

Andersen, D. J., Lindsley, D. H. & Davidson, P. M. (1993). QUILF; a Pascal program to assess equilibria among Fe–Mg–Mn–Ti oxides, pyroxenes, olivine, and quartz. *Computers and Geosciences* **19**, 1333–1350.

Barnea, E. & Mizrahi, J. (1973). A generalized approach to the fluid dynamics of particulate systems Part I. General correlation for fluidization and sedimentation in solid multiparticle systtems. *Chemical Engineering Journal* **5**, 171–189.

Barnes, S. J. (1986). The effect of trapped liquid crystallization on cumulus mineral compositions in layered intrusions. *Contributions to Mineralogy and Petrology* **93**, 524–531.

Bédard, J. H. (1989). Cumulus and post-cumulus processes in Monteregian and White Mountain complexes. *Abstracts, IAVCEI Meeting, Santa Fe, June 25–July 1.* Bureau of Mines, Socorro, New Mexico, p. 19.

Bédard, J. H. (1991). Cumulate recycling and crustal evolution in the Bay of Islands ophiolite. *Journal of Geology* **99**, 225–249.

Bédard, J. H. (2005). The roots of a flood basalt province: Expedition to Antarctica. *Elements* **1**(5), 316–317.

Bédard, J. H., Sparks, R. S. J., Renner, R., Cheadle, M. J. & Hallworth, M. A. (1988). Peridotite sills and metasomatic gabbros in the Eastern Layered Series of the Rhum complex. *Journal of the Geological Society, London* **145**, 207–224.

Bédard, J. H., Kerr, R. C. & Hallworth, M. A. (1992). Porous sidewall and sloping floor crystallization experiments using a reactive mush: implications for the self-channelization of residual melts in cumulates. *Earth and Planetary Science Letters* **111**, 319–329.

Bédard, J. H., Pagé, P. & Lissenberg, J. (2003). Melt transfer mechanisms in the lower ophiolitic crust: Examples from the Bay of Islands, Thetford-Mines, Betts Cove and Annieopsquotch. *EOS Transactions, American Geophysical Union* **84**, abstract F1540.

Bédard, J. H., Fleming, T., Hersum, T., Marsh, B., Mathez, E., Mukasa, S. B., Naslund, H. R. & Simon, A. (2005). Evidence for channelized transfer of residual melts and fluids in the Basement Sill, Ferrar Province, Antarctica. *American Geophysical Union Meeting, San Francisco,* Abstract V14C-05.

Blundy, J. D. & Holland, T. J. B. (1990). Calcic amphibole equilibria and a new amphibole–plagioclase geothermometer. *Contributions to Mineralogy and Petrology* **104**, 208–224.

Boudreau, A. E. (1987). Pattern formation during crystallization and the formation of fine-scale igneous layering. In: Parsons, I. (ed.) *Origins of Igneous Layering. NATO ASI Series C: Mathematical and Physical Sciences* **196**, 453–471.

Brey, G. P. & Köhler, T. (1990). Geothermobarometry in four-phase lherzolites. II. New thermobarometers, and practical assessment of existing thermobarometers. *Journal of Petrology* **31**, 1353–1378.

Campbell, I. H. (1987). Distribution of orthocumulate textures in the Jimberlana Intrusion. *Journal of Geology* **95**, 35–54.

Cawthorn, R. G. (2002). Delayed accumulation of plagioclase in the Bushveld Complex. *Mineralogical Magazine* **66**, 881–893.

Cawthorn, R. G., Sander, B. K. & Jones, I. M. (1992). Evidence for the trapped liquid shift effect in the Mount Ayliff Intrusion, South Africa. *Contributions to Mineralogy and Petrology* **111**, 194–202.

Chalokwu, C. I. & Grant, N. K. (1987). Reequilibration of olivine with trapped liquid in the Duluth complex, Minnesota. *Geology* **15**, 71–74.

Charrier, A. D. & Marsh, B. D. (2004). Sill emplacement dynamics from regional flow sorting of opx phenocrysts, Basement Sill, McMurdo Dry Valleys, Antarctica. *American Geophysical Union Meeting, Montréal*, abstract V42A-03.

Charrier, A. D. & Marsh, B. D. (2005). Sill emplacement dynamics: experimental textural modeling of a pulsing, cooling, particle-laden magma as applied to the Basement Sill, McMurdo Dry Valleys, Antarctica. *American Geophysical Union Meeting, San Francisco,* abstract V23A-0686.

Davis, R. H. & Acrivos, A. (1985). Sedimentation of noncolloidal particles at low Reynolds Numbers. *Annual Review of Fluid Mechanics* **17**, 91–118.

Dick, H. J. B., Meyer, P., Bloomer, S., Kirby, S., Stakes, D. & Mauwer, C. (1991). Lithostratigraphic evolution in an *in situ* section of oceanic layer 3. In: Von Herzen, R.P. & Robinson, P.T. *et al.* (eds) *Proceedings of the Ocean Drilling Program, Scientific Results, 118.* College Station, TX: Ocean Drilling Program, pp. 439–538.

Eales, H. V., Maier, W. D. & Teigler, B. (1991). Corroded plagioclase feldspar inclusions in orthopyroxene and olivine of the Lower and Critical Zones, Western Bushveld Complex. *Mineralogical Magazine* **55**, 479–486.

Elliot, D. H. (1992). Jurassic magmatism and tectonism associated with Gondwanaland break-up: an Antarctic perspective. In: Storey, B.C., Alabaster, T. & Pankhurst, R.J. (eds). *Magmatism and the Causes of Continental Break-Up, Geological Society, London, Special Publications* **68**, 165–184.

Elliot, D. H. (2000). Stratigraphy of Jurassic pyroclastic rocks in the Transantarctic Mountains. *Journal of African Earth Sciences* **31**, 77–89.

Elliot, D. H. & Fleming, T. H. (2000). Weddell triple junction: The principal focus of Ferrar and Karoo magmatism during initial breakup of Gondwana. *Geology* **28**, 539–542.

Elliot, D. H., Fleming, T. H., Haban, M. A. & Siders, M. A. (1995). Petrology and mineralogy of the Kirkpatrick basalt and Ferrar dolerite, Mesa Range region, North Victoria Land, Antarctica. In: Elliot, D. H. & Blaisdell, G. L. (eds) *Contributions to Antarctic Research IV. American Geophysical Union Antarctic Research Series*, pp. 103–141.

Fenistein, D. & van Hecke, M. (2003). Wide shear zones in granular bulk flow. *Nature* **425**, 256.

Fleming, T. H., Foland, K. A. & Elliot, D. H. (1995). Isotopic and chemical constraints on the crustal evolution and source signature

of Ferrar magmas, North Victoria Land, Antarctica. *Contributions to Mineralogy and Petrology* **121**, 217–236.

Geist, D., Boudreau, A., Garcia, M., Harpp, K., Mathez, E. & Marsh, B. (2005). Origin of mafic pegmatoids in the Dais Intrusion, Wright Valley, Antarctica. *American Geophysical Union Meeting, San Francisco*, abstract V14C-07.

German, R. M. (1989). *Particle Packing Characteristics*. Princeton, NJ: Metal Powder Industries Federation, 443 pp.

Greenspan, H. P. & Ungarish, M. (1982). On hindered settling of particles of different sizes. *International Journal of Multiphase Flow* **8**, 587–604.

Gunn, B. (1966). Modal and element variation in Antarctic tholeiites. *Geochimica et Cosmochimica Acta* **30**, 881–920.

Hall, R. P. & Hughes, D. J. (1987). Noritic dykes of southern West Greenland: early Proterozoic boninitic magmatism. *Contributions to Mineralogy and Petrology* **97**, 169–182.

Hamilton, W. & Hayes, P. T. (1965). Type Section of the Beacon Sandstone of Antarctica. *US Geological Survey Professional Papers* **456A**, 1–18.

Helz, R. T., Kirschenbaum, H. & Marinenko, J. W. (1989). Diapiric transfer of melt in Kilauea Iki lava lake, Hawaii: a quick, efficient process of igneous differentiation. *Geological Society of America Bulletin* **101**, 578–594.

Hergt, J. M., Peate, D. W. & Hawkesworth, C. J. (1991). The petrogenesis of Mesozoic Gondwana low-Ti flood basalts. *Earth and Planetary Science Letters* **105**, 134–148.

Hess, H. H. (1939). Extreme fractional crystallization of a basaltic magma; the Stillwater igneous complex. *Transactions of the American Geophysical Union*, **40**, *Part 3*, pp. 430–432.

Holness, M. B., Nielsen, T. F. D. & Tegner, C. (2007). Textural maturity of cumulates: A record of chamber filling, liquidus assemblage, cooling rate and large-scale convection in mafic layered intrusions. *Journal of Petrology* **48**, 141–157.

Hoshide, T., Obata, M. & Akatsuka,, T. (2006a). Crystal settling and crystal growth of olivine in magmatic differentiation—the Murotomisaki Gabbroic Complex, Shikoku, Japan. *Journal of Mineralogical and Petrological Sciences* **101**, 223–239.

Hoshide, T., Obata, M. & Akatsuka, T. (2006b). Magmatic differentiation by means of segregation and diapiric ascent of anorthositic crystal mush—the Murotomisaki Gabbroic Complex, Shikoku, Japan. *Journal of Mineralogical and Petrological Sciences* **101**, 334–339.

Hunter, R. H. (1987). Textural equilibrium in layered igneous rocks. In: Parsons, I. (ed.) *Origins of Igneous Layering. NATO ASI Series C: Mathematical and Physical Sciences* **196**, 473–503.

Irvine, T. N. (1980). Magmatic density currents and cumulus processes. *American Journal of Science* **280A**, 1–58.

Irvine, T. N. (1987). Layering and related structures in the Duke Island and Skaergaard Intrusions: Similarities, differences, and origins. In. In: Parsons, I. (ed.) *Origins of Igneous Layering. NATO ASI Series C: Mathematical and Physical Sciences***196**, 185–245.

Koyaguchi, T., Hallworth, M. A. & Huppert, H. E. (1993). An experimental study on the effects of phenocrysts on convection in magmas. *Journal of Volcanology and Geothermal Research* **55**, 15–32.

Kyle, P. R. (1980). Development of heterogeneities in the subcontinental mantle: Evidence from the Ferrar Group, Antarctica. *Contributions to Mineralogy and Petrology* **73**, 89–104.

Kynch, G. J. (1952). A theory of sedimentation. *Transactions of the Faraday Society* **48**, 166–176.

Marsh, B. D. (1981). On the crystallinity, probability of occurrence, and rheology of lava and magma. *Contributions to Mineralogy and Petrology* **78**, 85–98.

Marsh, B. D. (1988). Crystal capture, sorting, and retention in convecting magma. *Geological Society of America Bulletin* **106**, 1720–1737.

Marsh, B. D. (1996). Solidification fronts and magmatic evolution. *Mineralogical Magazine* **60**, 5–40.

Marsh, B. D. (2004). A magmatic mush column Rosetta Stone: The McMurdo Dry Valleys of Antarctica. *EOS Transactions, American Geophysical Union* **85**, 497.

Marsh, B. D., Hersum, T. G., Simon, A. C., Charrier, A. D. & Souter, B. J. (2005). Discovery of a funnel-like deep feeder zone for the Ferrar Dolerites, McMurdo Dry Valleys, Antarctica. *American Geophysical Union Meeting, San Francisco,* abstract V14C-03.

Martin, F. & Nokes, R. (1989). A fluid dynamical study of crystal settling in convecting magmas. *Journal of Petrology* **30**, 1471–1500.

McBirney, A. R. & Noyes, R. M. (1979). Crystallization and layering of the Skaergaard Intrusion. *Journal of Petrology* **20**, 487–554.

Naslund, H. R. & McBirney, A. R. (1996). Mechanisms of formation of igneous layering. In: (Cawthorn, R. G. Ed.). *Layered Intrusions. Developments in Petrology* **15**, 1–43.

Naslund, H. R., Bédard, J. H., Simon, A. & Mukasa, S. B. (2005). Small-scale modal layering in the Dais section of the Basement Sill, Ferrar Province, Antarctica. *American Geophysical Union Meeting, San Francisco,* abstract V13H04.

Nedderman, R. (1992). *Statics and Kinematics of Granular Materials*. Cambridge: Cambridge University Press.

Petford, N., Jerram, D. & Davidson, J. (2005). Slurry flow and structures formation in a magma mush: the Basement Sill, McMurdo Dry Valleys, Antarctica. *American Geophysical Union Meeting, San Francisco,* abstract V13H-05.

Pietranik, A., Koepke, J. & Puziewicz, J. (2006). Crystallization and resorption in plutonic plagioclase: Implications on the evolution of granodiorite magma (Gęsiniec granodiorite, Strzelin Crystalline Massif, SW Poland). *Lithos* **86**, 260–280.

Rubin, A. M. (1998). Dike ascent in partially molten rock. *Journal of Geophysical Research* **103**(B9), 20901–20919.

Schwandt, C. S. & McKay, G. A. (2006). Minor- and trace-element sector zoning in synthetic enstatite. *American Mineralogist* **91**, 1607–1615.

Simura, R. & Ozawa, K. (2006). Mechanism of crystal redistribution in a sheet-like magma body: Constraints from the Nosappumisaki and other shoshonite intrusions in the Nemuro Peninsula, Northern Japan. *Journal of Petrology* **47**, 1809–1851.

Storey, B. C., MacDonald, D. I. M., Dalziel, I. W. D., Isbell, J. L. & Millar, I. L. (1996). Early Paleozoic sedimentation, magmatism, and deformation in the Pensacola Mountains, Antarctica: The significance of the Ross Orogeny. *Geological Society of America Bulletin* **108**, 685–707.

Stump, E. (1995). *The Ross Orogen of the Transantarctic Mountains*. Cambridge: Cambridge University Press, 284 pp.

Sumita, I. & Manga, M. (2005). Rheology of suspensions and the emplacement of tongues of crystal-rich magma within sills. *American Geophysical Union Meeting, San Francisco,* abstract V23A-0678.

Tegner, C., Robins, B. & Sørensen, H. S. (1996). Crystallization from stratified magmas in the Honningsvåg Intrusive Suite, northern Norway: a reappraisal. *Mineralogical Magazine* **60**, 41–51.

Wager, L. R. & Deer, W. A. (1939). Geological investigations in East Greenland, Pt. III. The petrology of the Skaergaard Intrusion, Kangerdlugssuaq, East Greenland. *Meddelelser om Grønland* **105**, 1–352.

Wen, S. & Nekvasil, H. (1994). SOLVCALC: An interactive graphics program package for calculating the ternary feldspar solvus and for two-feldspar geothermometry. *Computers and Geosciences* **20**, 1025–1040.

Whitehead, J. A. & Kelemen, P. (1994). Fluid and thermal dissolution instabilities in magmatic systems. In: Ryan, M. P. (ed.) *Magmatic Systems*. New York: Academic Press, pp. 355–379.

Zhang, X., Luttinen, A. V., Elliott, D. H., Larsson, K. & Foland, K. A. (2003). Early stages of Gondwana breakup: The $^{40}Ar/^{39}Ar$ geochronology of Jurassic basaltic rocks from western Dronning Maud Land, Antarctica, and implications for the timing of magmatic and hydrothermal events. *Journal of Geophysical Research* **108**(B9), doi:10.1029/2001JB001070.

Zieg,, M. J. & Marsh, B. D. (2002). Crystal size distributions and scaling laws in the quantification of igneous textures. *Journal of Petrology* **43**, 85–101.